

1     **On Constructing Limits-of-Acceptability in Watershed Hydrology using Decision Trees**

2             Abhinav Gupta<sup>1</sup>, Rao S. Govindaraju<sup>2</sup>, Pin-Ching Li<sup>2</sup>, Venkatesh Merwade<sup>2</sup>

3             <sup>1</sup>Division of Hydrologic Sciences, Desert Research Institute, Las Vegas, NV, USA

4             <sup>2</sup>Lyles School of Civil Engineering, Purdue University, West Lafayette, IN, USA

5

6     Corresponding author: Abhinav Gupta ([abhinav.gupta@dri.edu](mailto:abhinav.gupta@dri.edu))

7

8

9     **THIS IS A PREPRINT AND IS UNDER REVIEW AT ADVANCES IN WATER**  
10  **RESOURCES.**

11

## 12 Abstract

13 A hydrological model incurs three types of uncertainties: measurement, structural and parametric  
14 uncertainty. For instance, in rainfall-runoff models, measurement uncertainty exists due to errors  
15 in measurements of rainfall and streamflow data. Structural uncertainty exists due to errors in  
16 mathematical representation of hydrological processes. Parametric uncertainty is a consequence  
17 of our inability to measure effective model parameters, limited data available to calibrate model  
18 parameters, and measurement and structural uncertainties. Measurement and structural  
19 uncertainties are inseparable without additional information about measurement uncertainties. The  
20 existence of these predominantly epistemic uncertainties makes the model inference difficult.  
21 Limits-of-acceptability (LOA) framework has been proposed in the literature for model inference  
22 under a rejectionist framework. LOAs can be useful in model inference if they reflect the effect of  
23 errors in rainfall and streamflow measurements. In this study, the usefulness of quantile random  
24 forest (QRF) algorithm has been explored for constructing LOAs. LOAs obtained by QRF were  
25 compared to the uncertainty bounds obtained by rating-curve analysis and the LOAs obtained by  
26 runoff ratio method. Rating curve analysis yields uncertainty in streamflow measurements only  
27 and the runoff ratio method is expected to reflect uncertainty in rainfall and streamflow volume  
28 measurements. LOAs obtained by using QRF were found to envelop the uncertainty bounds due  
29 to streamflow measurement errors. The variation of width of LOAs was similar for QRF and runoff  
30 ratio methods. Further, QRF LOAs were scrutinized in terms of their ability to reflect the effect of  
31 rainfall uncertainty, both qualitatively and quantitatively. Results indicate that QRF LOAs reflect  
32 the effect of rainfall uncertainty: increase in standard deviation with increase in mean streamflow  
33 values and decrease in coefficient of variation with increase in mean streamflow values. A  
34 mathematical analysis of the LOAs obtained by the QRF method is presented to provide a  
35 theoretical foundation.

36 **Keywords:** Hydrological model, Uncertainty, Machine learning, Runoff ratio, Limits-of-  
37 Acceptability, Model validation

## 38 1. Introduction

### 39 1.1 Background

40 In a generic hydrologic model,

$$41 \mathbf{y} = g(\mathbf{x}, \boldsymbol{\theta}) + \boldsymbol{\delta} + \boldsymbol{\epsilon}, \quad (1)$$

42  $\boldsymbol{\delta}$  and  $\boldsymbol{\epsilon}$  denote the *effect* of structural and measurement errors (Beven, 2005) in the estimation of  
43 time series of observed hydrologic variables (e.g., streamflow)  $\mathbf{y}$  by the approximate model  $g$ .  
44 Here  $\mathbf{x}$  denotes model inputs such as rainfall and temperature, and  $\boldsymbol{\theta}$  denotes the set of model  
45 parameters. Measurement errors refer to errors in measurements of rainfall and streamflow, while  
46 structural errors refer to errors in the mathematical representation of hydrologic processes. Given  
47 a parameter set  $\boldsymbol{\theta}^s$ , the structural and measurement errors are estimated based on the residual time  
series  $\mathbf{y} - g(\mathbf{x}, \boldsymbol{\theta}^s)$ .

48 If an appropriate probability distribution over  $\boldsymbol{\delta}$  and  $\boldsymbol{\epsilon}$  may be assumed, the parameters of the  
49 distributions along with hydrologic model parameters can be obtained by using Bayes theorem  
50 (Kennedy and O'Hagan, 2001). However, the use of formal probability distributions has its own  
51 challenges (Beven and Smith, 2015). Often, a probability distribution over the *sum* of  $\boldsymbol{\delta}$  and  $\boldsymbol{\epsilon}$  is  
52 assumed, such as Gaussian or generalized Gaussian (Schoups and Vrugt, 2010; Ammann et al.,  
53 2019; Smith et al., 2015). But the residual time series can yield only an aggregate estimate of the

54 effect of measurement and structural errors, that is, the quantities  $\delta$  and  $\epsilon$  are individually  
55 unidentifiable (Renard et al., 2010; Renard et al., 2011; Brynjarsdottir and O'Hagan, 2014).  
56 Separate identification of structural and measurement errors is required to determine what part of  
57 modeling exercise needs to be addressed to reduce total uncertainty, the data or the model (e.g.,  
58 Reichert and Mieleitner, 2009) and to facilitate rejection of bad models.

59 To identify structural uncertainty in a model, strong prior information about measurement  
60 uncertainties is required (Renard et al., 2010; McMillan et al., 2012; Brynjarsdottir and O'Hagan,  
61 2014; McMillan et al., 2018), and this information should be obtained before calibration and  
62 independent of the hydrologic model being used. Given information about measurement  
63 uncertainty and the residual time series corresponding to a model (or model parameter), a Bayesian  
64 characterization of structural uncertainty is possible in the sense that one can obtain a probabilistic  
65 estimate of the effect of structural uncertainty conditioned upon each possible realization of rainfall  
66 (and other inputs) and streamflow time series. Priors over measurement uncertainty are typically  
67 constructed by making aleatoric assumptions about the nature of these errors. For example, one  
68 can obtain information about random measurement uncertainty in streamflow by using rating curve  
69 analysis (Kiang et al., 2018; Overleir et al., 2009; Reitan and Overleir, 2009; Le Coz et al., 2014)  
70 or other probabilistic methods (de Oliveira and Vrugt, 2022). But epistemic uncertainties in  
71 streamflow, such as those introduced by extrapolation of rating curve to gauge heights well above  
72 the observations, may not be knowable. Reliable information about rainfall measurement  
73 uncertainty cannot be obtained in most situations. For instance, one may estimate the uncertainty  
74 in areal average rainfall by assuming that this uncertainty is dominated by spatial variability of  
75 rainfall and neglecting temporal errors and biases (Moulin et al., 2009; Renard et al., 2011). Spatial  
76 variability can be modeled using a statistical model such as Kriging, provided that enough data to  
77 estimate the parameters of the variogram are available. This is further complicated as the  
78 parameters of the variogram will change from event to event in unknown ways. Precipitation data  
79 also incur timing errors which can be significant if the precipitation gauges are sparse or are located  
80 outside the watershed.

81 If the observed data seem to violate the principle of mass balance (e.g., Beven and Westerberg,  
82 2011), one may expect errors in the measurements of either rainfall data, or streamflow data, or  
83 both. Such time-periods in rainfall-runoff time series are referred to as disinformative (Beven and  
84 Westerberg, 2011) which should be discarded before model fitting. A disinformative event can  
85 introduce bias in the modeling effort because it violates mass balance, and also because it affects  
86 the antecedent conditions for subsequent events (Beven and Smith, 2015). Disinformative periods  
87 in a rainfall-runoff dataset may be identified as the ones with exceptionally high and low runoff  
88 ratios (Beven and Westerberg, 2011) where runoff ratio of an event is defined as the ratio of total  
89 event streamflow to total event rainfall. What is an exceptionally high or low value of runoff ratio  
90 may be determined using the knowledge about the rainfall-runoff response of the watershed.  
91 Several other attempts have been made to characterize the uncertainty in hydrologic data and  
92 hydrologic modeling (e.g., Kuczera and Parent, 1998; Kavetski et al., 2006a; Kavetski et al.,  
93 2006b; Gabellani et al., 2007; McMillan et al., 2018), but it still remains an unsolved problem  
94 because of dominantly epistemic nature of these errors. Recently, Gupta and Govindaraju (2022)  
95 noted that several methods have been proposed for uncertainty analysis in hydrology but there is  
96 no consensus on which method should be used.

97 Recently, the runoff ratio method has been proposed to construct limits-of-acceptability (LOA)  
98 bounds on streamflow that could then be used to identify behavioral models (Beven, 2019). A

99 model (or a model parameter set) is considered behavioral if the streamflow simulated by it falls  
100 within the LOA at some predefined timesteps (Beven et al., 2022) depending on the purpose of  
101 modeling. It is clear that LOA should be such as to *encompass* the uncertainty due to measurement  
102 errors in rainfall and streamflow. Thus, a model that properly accounts for streamflow dynamics  
103 within the margin of measurement errors would not be rejected and will be considered behavioral.

104 LOAs have also been defined using flow duration curves (FDCs; Westerberg et al., 2011). In this  
105 method, measurement uncertainty over streamflow time series is constructed using rating-curve  
106 analysis. Measurement uncertainty in streamflow is converted to an uncertainty bound over FDC.  
107 A model (or model parameter set) is considered behavioral if the FDC simulated by it falls into  
108 the FDC uncertainty bound. However, this method only compares the probability distribution of  
109 observed and simulated streamflows and removes the temporal information from the streamflow  
110 time series. Also, it does not account for rainfall measurement errors. In fact, most of the methods  
111 to derive LOAs are based on streamflow uncertainty only and neglect rainfall uncertainty (e.g.,  
112 Kruger et al., 2010; Coxon et al., 2014). To the best of author's knowledge, the runoff ratio method  
113 is the only method that constructs LOAs while acknowledging uncertainty in both streamflow and  
114 rainfall measurements. The runoff ratio method also has some limitations as discussed below.

115 Fundamentally, the LOA method has been proposed in a rejectionist framework (Beven and Lane,  
116 2019), which makes it different from Bayesian method wherein no models are explicitly rejected.  
117 Frequentist statistics also provides a model rejection framework such as the likelihood ratio test  
118 (Neyman and Pearson, 1933), Fisherian hypothesis testing (Fisher, 1973) and, more recently,  
119 evidential testing (Royall, 1997; Lele, 2004). But these methods are based on aleatoric assumptions  
120 (as are Bayesian methods) about various uncertainties and, therefore, are difficult to justify in  
121 hydrologic applications. There have been a relatively few attempts in hydrology to use rigorous  
122 frequentist methods for model inference (but see Pande, 2013a; Pande, 2013b). The LOA  
123 framework provides an alternative to these statistical frameworks, which combines the elements  
124 of Bayesian theory (parameter update as the models are tested against more data) and frequentist  
125 statistics (model rejection). LOA can also be applied in a purely Bayesian framework by defining  
126 an appropriate LOA based likelihood function (e.g., Krueger et al., 2010). The aim of this study  
127 was to explore the potential of using machine learning algorithms called decision tree (DT) and,  
128 in particular, quantile random forest (QRF) in constructing LOAs in gauged and ungauged  
129 locations.

## 130 *1.2 Runoff ratio method, and decision trees*

131 In runoff ratio method, the rainfall and streamflow time series are divided into separate rainfall-  
132 runoff events. Then, the rainfall-runoff events with similar characteristics are pooled together. The  
133 main idea is that the two similar events should have similar runoff ratios. Of course, no two events  
134 are exactly similar, and there would be some differences in runoff ratios. But the large differences  
135 can be (at least partly) attributed to either rainfall measurement errors, or streamflow measurement  
136 errors, or both. The differences between runoff-ratio of two similar events can also occur because  
137 of epistemic variability. Multiplying a *zero-loss streamflow* event with runoff ratios of all the  
138 similar events would result in an ensemble of corresponding streamflow hydrographs. Zero-loss  
139 streamflow can be obtained by dividing the observed hydrograph by the corresponding runoff  
140 ratio. Beven (2019) suggested that the upper and lower bounds of these hydrographs be used as  
141 LOA over the rainfall-runoff event in question. This method is described in more detail below.

142 The advantage of the runoff ratio method is that it allows to define distribution of streamflow  
143 hydrographs for a given rainfall event and antecedent conditions based on available data. One of  
144 the limitations of this method is that it is applicable to flashy watersheds only (Beven, 2019). Also,  
145 this method cannot account for potential timing errors in precipitation – it only accounts for errors  
146 in precipitation volume and can be applied only at event timescale. Further, this method cannot be  
147 used to construct LOAs at ungauged locations where streamflow data are unavailable for  
148 computing runoff ratios.

149 These limitations can be addressed by using an ML method, while retaining the advantage of the  
150 runoff ratio method. A direct mapping between relevant watershed attributes, meteorological data,  
151 and streamflow can be created by using a Machine learning (ML) algorithm (e.g., Govindaraju,  
152 2000; Zhang and Govindaraju, 2000; Zhang and Govindaraju, 2003; Iorgulescu and Beven, 2004;  
153 Shortridge et al., 2016; Kratzert et al., 2020). ML can be particularly useful in constructing LOAs  
154 for baseflow dominated watersheds where runoff ratio method is not applicable and to construct  
155 LOAs at ungauged locations. Further, the ML approach allows defining LOAs at the scale of  
156 available data rather than event timescale. As discussed below, ML algorithms called decision  
157 trees (DTs) are particularly well-suited in this regard.

158 Another advantage of the ML approach is that the data from several watersheds may be used to  
159 train the model and define LOAs. Data from different watersheds, however, may introduce  
160 disinformation because of watershed-specific epistemic uncertainties (Beven, 2020). But the  
161 hydrologically relevant information available from other watersheds may still be useful, especially  
162 when LOAs are to be constructed for an ungauged watershed. An ML algorithm such as DT will  
163 be able to identify hydrologically similar watersheds based on available watershed characteristics,  
164 albeit that watersheds characteristics are typically represented by spatially averaged indices  
165 neglecting the spatial distribution of the various characteristics which may have important control  
166 over hydrological behavior. Thus, DTs are natural candidates to consider for constructing LOAs  
167 as discussed below.

168 The uncertainties in hydrologic data are predominantly epistemic, which may change from event  
169 to event in unknown ways. This means that the true statistical behavior of uncertainties will not be  
170 generally represented by the available data. Therefore, DT would either overpredict or  
171 underpredict the effect of measurement errors. While overprediction is acceptable, underprediction  
172 may be problematic in many applications. Therefore, one needs to allow for outliers while  
173 validating the models using the LOA method (as in Beven et al., 2022). Further, the DT model  
174 would compensate for systematic biases. These systematic errors cannot be detected by a statistical  
175 approach. A bias term can be introduced in statistical models, but these models would not be able  
176 to differentiate between the bias in the data and the bias in the model simulations.

177 The classical method of finding uncertainty in the measurement of a phenomenon is to repeat the  
178 measurement process several times under identical conditions. The repeated sampling method,  
179 however, is impossible for the measurements of environmental phenomena such as rainfall and  
180 streamflow (McMillan et al., 2012). But an approximate repeated sampling method may be  
181 implemented for environmental measurements. The main idea is to estimate the effect of  
182 measurement uncertainty using observations of rainfall-streamflow events under *similar*  
183 conditions across several different events and/or several different watersheds. The runoff ratio and  
184 DT methods can be thought of as approximate repeated sampling techniques.

185 Once the LOAs are obtained, either formal (Kuczera et al., 2006) or informal Bayesian (Liu et al.,  
186 2009; Krueger et al., 2010; Beven and Lane 2021) methodologies may be used for subsequent  
187 uncertainty analysis. In informal methods, one may define behavioral models (and model  
188 parameters) as ones that yield streamflow time series within the LOA. Thus, all the models with  
189 an inferior structure will be eventually rejected as more and more data are used (at least that is the  
190 expectation). One can also use the apparatus of formal Bayesian theory for model (or parameter)  
191 inference using the LOAs in Approximate Bayesian Computation framework (Nott et al., 2012;  
192 Sadgeh and Vrugt, 2013; Vrugt and Sadgeh, 2013; Vrugt and Beven, 2018).

### 193 *1.3 Objectives*

194 The objective of this study is to develop a method for constructing LOAs that can account for both  
195 precipitation and streamflow measurement errors and can be used for ungauged catchments. In  
196 this study, we ask if a variant of DT called quantile random forest (QRF) can be used to construct  
197 meaningful LOAs. A second question is if the LOAs obtained by QRF algorithm are comparable  
198 to the LOAs obtained by the runoff ratio method of Beven (2019).

199 The novelty of this study lies in using QRF model to construct LOAs that account for *measurement*  
200 *uncertainty* (not predictive uncertainty) based on available data. To address the objective of this  
201 study, uncertainty bounds obtained by QRF model are scrutinized to check if they can be used as  
202 LOAs. The uncertainties in real world data are, however, unknown; therefore, it is impossible to  
203 check if the uncertainty bounds obtained by any method represent true uncertainties. However,  
204 some characteristics of the uncertainties can be obtained by using statistical methods based on  
205 aleatoric assumptions; we test whether the QRF estimated LoAs reflect the effect of these  
206 uncertainties.

207 Further, this paper presents a mathematical analysis of the proposed hypothesis. The goal of the  
208 mathematical analysis is (1) to show how decision trees such as QRF can be used to encompass  
209 measurement uncertainties due to errors in rainfall and streamflow measurements, and (2) to  
210 clarify the logic and assumptions behind the proposed method.

211 In Section 2, the theory behind DTs and QRF algorithm are discussed along with the methodology  
212 to empirically test the proposed method. Section 3 discusses the results of the study. In Section 4,  
213 presents a brief mathematical analysis of the QRF method in terms of defining LOAs. Section 5  
214 concludes the paper.

## 215 **2. Theory and methodology**

### 216 *2.1 Study area, data, and the models developed*

217 In this study, data from Ohio river basin (ORB) were used to calibrate and validate the QRF model.  
218 This basin contains 431 USGS streamflow stations (Figure 1). The streamflow data were  
219 downloaded from USGS website for all the 431 stations. Data for these watersheds are available  
220 from water year 2011 to 2020. Total drainage area of each USGS station was delineated on the  
221 30m × 30m resolution digital elevation model (Archuleta et al., 2017; U.S. Geological Survey,  
222 The National Map, 2017) by using the ArcHydro toolbox. For each of the drainage areas, predictor  
223 variables (listed in Table 1) were computed or collected. Climate data were collected over the  
224 study area from Historical Climate Network (HCN) stations available at National Centers for  
225 Environmental Information (NCEI) website.

226 To test the capability of the QRF model in capturing rainfall and streamflow measurement  
 227 uncertainties, data from St. Joseph River Watershed (SJRW) were used as test cases. SJRW is  
 228 located just above the ORB in Northwest as indicated in Figure 1 (see also Figure B1 in Appendix  
 229 B). Specifically, QRF models were used to generate LOAs at four USGS streamflow stations  
 230 located in SJRW.

231 Three kinds of QRF models were developed:

232 (1) Gauged-single scenario: In this case, four QRF models were developed for each of the four  
 233 SJRW watersheds using data from the watershed where the LOAs were to be constructed. For  
 234 example, to construct LOAs at station 04180500, the data from only this station were used to  
 235 train the QRF model. These models are referred to as “gauged-single models”.

236 (2) Gauged scenario: In this case, a QRF model was trained using data from both the ORB and the  
 237 four SJRW watersheds. The model thus trained is referred to as “gauged model”. Three kinds  
 238 of models were developed in this scenario: (2a) QRF was trained using data from all the  
 239 training watersheds (referred to ‘gauged all’), (2b) QRF was trained using data from the 4 most  
 240 similar watersheds to watershed where LOAs are to be constructed (referred to ‘gauged 4’),  
 241 and (2c) QRF was trained using the data from the 20 most similar watersheds (referred to  
 242 ‘gauged 20’).

243 (3) Ungauged scenario: In this case, a QRF model was trained using data only from the ORB  
 244 watersheds without using the SJRW data. The model thus trained will be referred to as  
 245 “ungauged model”. Out of the 431 ORB stations, 80% of the stations were fixed for the  
 246 calibration of QRF and the remaining stations were fixed for validation.

247 Similar watersheds in the ‘gauged scenario’ were selected based on the watershed static attributes  
 248 and mean climate (mean precipitation and temperatures). The first two scenarios allow us to test  
 249 the usefulness of QRF approach in constructing LOAs at a gauged location and the third scenario  
 250 allows us to test the usefulness of the approach at ungauged location. The comparison of the first  
 251 two and the third scenario allows to test the usefulness of data across different watersheds in  
 252 constructing LOAs.

253  
 254 Table 1. Predictor variables in machine learning models to estimate streamflow time series at a  
 255 station in a river-network. Exploratory statistics in the third column represent (minimum,  
 256 maximum, median, and mean)

Predictor variable	Description	Exploratory Statistics
Drainage area (Km <sup>2</sup> )	Cumulative drainage area of streamflow station	(7.74, 250260, 624, 4187)
Impervious Area*(%)	Percentage of impervious area	(1.92, 7.74, 6.36, 6.44)
Sand content**(%)	Percentage of sand content	(6.34, 49.61, 20.97, 19.78)
Clay content (%)	Percentage of clay content	(15.88, 45.12, 26.03, 27.58)
Conductivity (µm s <sup>-1</sup> )	Average hydraulic conductivity of the drainage area	(0.01, 77.22, 0.19, 3.51)
Permeability (cm hr <sup>-1</sup> )	Average permeability of the drainage area	(1.02, 15.09, 3.87, 4.82)
Rainfall***	Total daily rainfall during current and previous 1, 7, and 30 days	–
Snowfall	Total Daily snowfall during current and previous 1 and 30 days	–
Snow depth	Daily snow depth during current and previous 1 and 30 days	–

Temperature

Average daily maximum and minimum temperature at –  
current day

\* Land-use data were collected from NLCD database

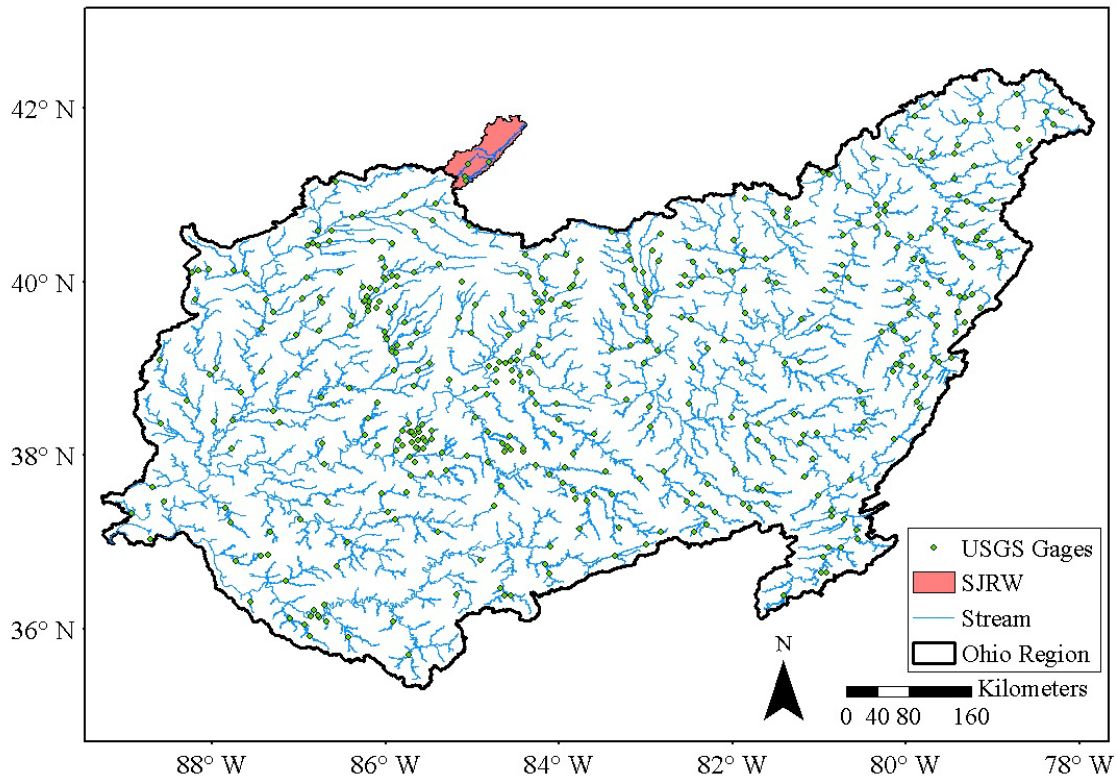
\*\* Soil data were collected from STATSGO database

\*\*\* Climate data were collected from Global Historical Climatology Network (GHCN) database

257

258

259



260 Figure 1. Ohio river basin (ORB) and USGS streamflow stations (green dots). The watershed  
261 with red background is St. Joseph River Watershed (SJRW).

262

263 Table 2. List of USGS stations used for rating-curve analysis and application of runoff ratio  
264 method. These stations are located St. Joseph River Watershed (SJRW).

USGS station	Drainage Area (km <sup>2</sup> )
04180500	2745.40
04180000	699.30
04179520	233.62
04178000	1579.90

## 265 2.2 Machine learning models to map predictor variables to streamflow

266 The main idea behind ML algorithms is to create a mapping between predictor and response  
267 variables (Friedman et al., 2001, chap. 2). For most watershed scale rainfall-runoff models, the set  
268 of predictor variables constitutes meteorological data, soil data, land-use data, etc. (Table 1), and



269 the response variable typically is streamflow time series. Available data are divided into calibration  
 270 and validation sets. The samples contained in calibration set are used to create a mapping such that  
 271 a loss function, which is a function of the mapping, is minimized, and the samples contained in  
 272 validation set are used to test the generalizability of the created mapping.

273 In this study, an ML algorithm called quantile random forest (QRF) was used to create a mapping  
 274 between predictor and response variables (Brieman, 2002). The basic building block of QRF is  
 275 another ML algorithm called regression trees (Friedman et al., 2001, chap. 9; Iorgulescu and  
 276 Beven, 2004). Regression trees create a non-linear mapping between predictor variables and  
 277 response variables. In this method, the space of predictor variables is divided into  $S$  (contiguous)  
 278 subregions, and in each subregion, the response variable is approximated by a unique function.

279 Let the set containing predictor and response variables be denoted by  $\mathcal{D}$ . Each element of  $\mathcal{D}$   
 280 represents a calibration/training sample. Let the  $i^{\text{th}}$  calibration sample be denoted by  $(\mathbf{x}_i, y_i)$ , then  
 281  $\mathcal{D} = \{(\mathbf{x}_1, y_1), (\mathbf{x}_2, y_2), \dots, (\mathbf{x}_N, y_N)\}$  where  $N$  is the total number of calibration samples. The  
 282 vector  $\mathbf{x}_i$  is a  $p$ -vector where  $p$  denotes the number of predictor variables, that is,  $\mathbf{x}_i =$   
 283  $(x_{i1}, x_{i2}, \dots, x_{ip})$ , and  $y_i$  is a scalar that denotes the response variable corresponding to the  $i^{\text{th}}$   
 284 sample. In this study, the  $i^{\text{th}}$  response variable is streamflow at the outlet of a watershed at a  
 285 particular time-step. The  $i^{\text{th}}$  predictor vector includes static watershed attributes and  
 286 meteorological data at multiple lags (Table 1). The regression tree is created using an iterative  
 287 procedure. In the first iteration, the set  $\mathcal{D}$  is divided into two (or more) subsets based on a randomly  
 288 selected  $j^{\text{th}}$  predictor variable. Let the two subsets be denoted by  $\mathcal{D}_{11}$  and  $\mathcal{D}_{12}$ , then

$$\begin{aligned} \mathcal{D}_{11} &= \{(\mathbf{x}_i, y_i) | x_{ij} < x_{j,\text{thresh}}\}, \\ \mathcal{D}_{12} &= \mathcal{D} \setminus \mathcal{D}_{11}, \end{aligned} \quad (2)$$

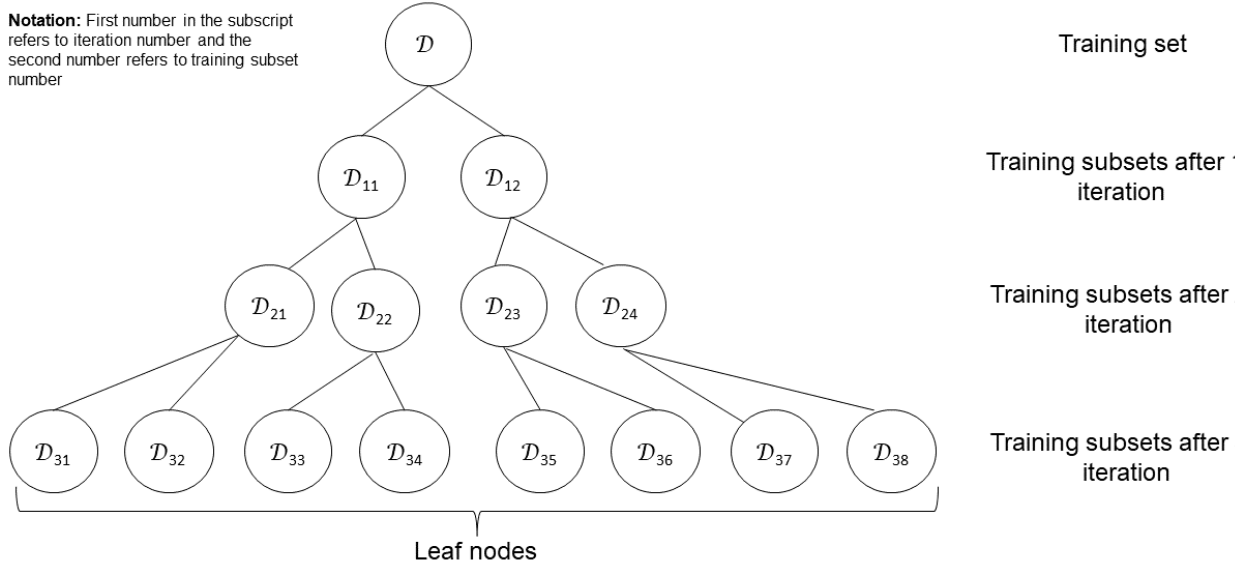
289 where  $x_{j,\text{thresh}}$  denotes a randomly chosen threshold for  $j^{\text{th}}$  predictor variable. In the second  
 290 iteration, the subsets  $\mathcal{D}_{11}$  and  $\mathcal{D}_{12}$  are further divided into smaller subsets, and so on for subsequent  
 291 iterations. At the end of the iterative procedure,  $S$  smaller subsets of  $\mathcal{D}$  are obtained, and each  
 292 subset occupies a distinct region of the predictor space. Thus, the regression tree algorithm divides  
 293 the predictor space into  $S$  contiguous subregions. This method is referred to as regression trees  
 294 because the process of division of training samples into  $S$  subsets can be visualized as creating a  
 295 tree (Figure 2, see also Friedman et al., 2001, pp. 268). The tree grows deeper with each iteration.  
 296 Therefore, the number of iterations is also referred to as tree depth. Typically, a maximum value  
 297 of tree depth,  $d$ , is assigned to avoid overfitting. The subsets obtained in the last iteration are also  
 298 referred to as leaf nodes. It is clear that there is a relationship between the number of leaf nodes  $S$   
 299 and maximum tree depth  $d$ : an increase in  $d$  implies an increase in  $S$ . Note that once the tree is  
 300 created, each subregion can be identified by a set of rules on predictor variables.

301 After the tree is created, response of a sample with predictor vector  $\mathbf{x}$  is obtained as follows. The  
 302 first step is to identify the subregion of the predictor space to which the vector  $\mathbf{x}$  belongs. Suppose  
 303 that  $\mathbf{x}$  belongs to the  $i^{\text{th}}$  subregion corresponding to  $i^{\text{th}}$  training subset denoted by  $S_i$ . Then the  
 304 response variable corresponding to  $\mathbf{x}$  is estimated as the average response of calibration samples  
 305 contained in  $S_i$

$$\hat{y}(\mathbf{x}) = \frac{1}{L_i} \sum_{j=1}^{L_i} y(\mathbf{x}_j), \quad (3)$$

306 where  $L_i$  denotes the number of samples in  $S_i$ . Regression trees are developed so that the sum of  
 307 square errors between observed and estimated responses is minimized (with some regularization  
 308 to avoid over-fitting). The averaging of data in the leaf node, however, neglects the variability in  
 309 the data. Therefore, not just the average but the entire distribution  $y(\mathbf{x}_j)$  for  $\mathbf{x}_j \in S_i$  were used to  
 310 construct LOAs as explained below.

311



312 Figure 2. Illustration of regression tree. In this hypothetical example, only three iterations were  
 313 carried out to divide the training set into smaller subsets.

314 The method of regression trees is particularly suitable for the purpose of creating LOAs because  
 315 it mimics the function of an approximate repeated sampler by grouping similar calibration samples  
 316 (similarity in predictor space) together based on several watershed attributes, thus enabling the  
 317 accounting of measurement uncertainty due to errors in response and predictor variables.  
 318 Regression trees have to be regularized to avoid overfitting; therefore,  $B$  regression trees are  
 319 developed instead of a single one. Each of the  $B$  regression trees is created by randomly drawing  
 320  $K$  samples by bootstrapping from the calibration set  $\mathcal{D}$ . This, yields an ensemble  $Y(\mathbf{x}) =$   
 321  $\{\hat{y}_1(\mathbf{x}), \hat{y}_2(\mathbf{x}), \dots, \hat{y}_B(\mathbf{x})\}$  of streamflow estimates corresponding to the predictor variable  $\mathbf{x}$  where  
 322 the  $b^{\text{th}}$  estimate  $y_b(\mathbf{x})$ , obtained by Eq. (3), corresponds to the  $b^{\text{th}}$  tree. The average of values in  
 323  $Y(\mathbf{x})$  is taken as the final estimate. This method is known as random forest (RF). In this study, the  
 324 RF algorithm was used to create a mapping between predictor variables (listed in Table 1) and  
 325 streamflow, and the streamflow in each subregion of the predictor space was estimated as the  
 326 average streamflow of calibration samples in that subregion (Eq. 3). But as mentioned above,  
 327 taking averages of data in the leaf node neglects the variability in the leaf node which might contain  
 328 important information about uncertainties. Therefore, quantile random forest (QRF) technique was  
 329 used to construct LOAs, where quantiles instead of averages are computed. In this technique, the  
 330 ensemble  $Y_{\text{QRF}}$  is constructed by using the entire distribution of data in leaf nodes. If a given  
 331 predictor, say  $\mathbf{x}$ , falls into the  $i^{\text{th}}$  leaf node of the  $b^{\text{th}}$  tree, denoted by  $S_i^b$ , then the distribution of  
 332 response variable in  $S_i^b$  can be represented as:

$$Y^b(\mathbf{x}) = \{y_j | y_j \in S_i^b, \}. \quad (4)$$

333 Thus, we will have a distribution  $Y^b$  for each tree. Now, the data from each  $Y^b$  can be combined  
 334 to form an ensemble  $Y_{\text{QRF}}(\mathbf{x})$

$$Y_{\text{QRF}}(\mathbf{x}) = \{y_j | y_j \in Y^b, b = 1, 2, \dots B\}. \quad (5)$$

335 Note that the  $y_j$  values contained in  $Y_{\text{QRF}}$  are observed values not the estimates. QRF estimates  
 336 different quantiles of the response for a given  $\mathbf{x}$  by treating  $Y_{\text{QRF}}$  as the distribution of response. In  
 337 this study, 2.5<sup>th</sup> and 97.5<sup>th</sup> percentiles obtained by QRF were used as lower and upper LOAs. We  
 338 found that these percentiles were typically adequate for constructing LOAs in the sense that most  
 339 of the observations were enveloped by the LOAs but a few flow values could not be enveloped.  
 340 Therefore, in practical application more extreme percentiles might be appropriate for creating  
 341 LOAs.

342 If the premise ‘the ensemble of estimated streamflow represents only measurement uncertainty’  
 343 were true, then in the absence of measurement errors the different streamflow estimates in the  
 344 ensemble would be (approximately) identical. In practice, however, even in the absence of  
 345 measurement errors, the streamflow estimates in the ensemble would be different because of  
 346 several reasons:

- 347 (1) Imperfections in creating the regression trees: These imperfections include selection of  
 348 appropriate values of  $B$  (number of regression trees) and  $S$  (number of leaf nodes). A large  
 349 value of  $S$  (or large value of maximum tree depth  $d$ ) may result in an over-estimation of  
 350 measurement errors and conversely for a small value of  $S$  (or small value of  $d$ ). In this  
 351 study, optimal values of  $B$  and  $d$  along with minimum number of samples in a leaf node  
 352 were estimated by computing the out-of-bag (OOB) error (Breiman, 1996). The OOB error  
 353 is the prediction error of calibrated RF from the left-out training set. An early stopping  
 354 method searches for the optimal values of these parameters with the minimal OOB error.
- 355 (2) Small calibration set which is inadequate to represent the population of measurement  
 356 errors : Calibration sets should be large enough such that the variability in measurement  
 357 errors (in rainfall and streamflow) is captured. In this study, data from a total of 431 ORB  
 358 stations plus 4 SJRW stations were used, out of which data from a total of 344 stations  
 359 were used for calibration.
- 360 (3) The set of predictor variables used to train the ML algorithm is incomplete: If a relevant  
 361 predictor variable is missed in the set of predictor variables, the uncertainty bound yielded  
 362 by QRF would also contain structural errors. The predictor variables used in this study are  
 363 listed in Table 1. Though these predictors variable are incomplete; they are still good  
 364 enough to estimate the streamflow time series accurately in many watersheds, as evident  
 365 by high NSE for some of the test stations shown in the results section.

366 Even after taking all the precautions, the LOAs created by QRF method would still contain  
 367 structural errors. QRF would be able to construct better LOAs as the sample size increases. When  
 368 the LOAs are to be constructed at a gauged location, the longer length of data at the location will  
 369 be more important than the data from other watersheds. But data from other watersheds would be  
 370 the only option when LOAs are to be constructed at an ungauged location.

371 The LOAs obtained by QRF were compared against the bounds obtained over streamflow  
 372 measurements uncertainty which in turn were obtained by rating curve analysis. If the LOAs  
 373 obtained by QRF indeed reflect the effects of measurement uncertainties in rainfall and  
 374 streamflows, these should envelop the uncertainty bound obtained by rating curve analysis. Also,  
 375 we compared the bounds obtained by runoff ratio method to the bounds obtained by QRF method.  
 376 Analysis of rating curve and runoff ratio were carried out at the four USGS streamflow gauging  
 377 stations within SJRW as indicated in Table 1. SJRW is located just above the ORB in Northeast  
 378 of ORB as indicated in Figure 1.

379 Moreover, the QRF LOA should also reflect the effects of measurement uncertainty in rainfall. In  
 380 this study, the measurement uncertainty in areal average rainfall was obtained using an empirical  
 381 approach. One challenge is that the rainfall uncertainty bounds cannot be directly compared to the  
 382 LOAs since rainfall is processed through the watersheds in a highly non-linear fashion before it  
 383 reaches the watershed outlet. There is no exact way of translating measurement uncertainty in  
 384 rainfall to streamflow space: this would require a perfect hydrological model, free of structural  
 385 errors. If we had a perfect hydrological model, measurement uncertainty could actually be  
 386 estimated by using this model and analyzing the residuals as discussed in the Introduction.  
 387 Therefore, in this study, the various realizations of rainfall were processed through the SCS curve-  
 388 number ( $CN$ ) formula for different value of  $CN$  to get an estimate of excess rainfall. Subsequently,  
 389 coefficient of variation of streamflow ( $CV_Q$ ) were compared to the coefficient of variation of excess  
 390 rainfall time series ( $CV_R$ ).

### 391 2.3 Rating curve analysis to quantify uncertainties in measured streamflow

392 The streamflow at a river cross-section is estimated using the observed relationship between  
 393 measured gage heights at the cross-section and corresponding measured discharges; this  
 394 relationship is referred to as rating curve (Herschy, 1993). Commonly, a rating curve is modeled  
 395 as multiple power law segments (Le Coz et al., 2014):

$$\log(Q_r(h)) = \begin{cases} 0, & h \leq h_{0,1}, \\ \log a_1 + b_1 \log(h - h_{0,1}), & h_{0,1} \leq h \leq h_{s,1}, \\ \log a_2 + b_2 \log(h - h_{0,2}), & h_{s,1} \leq h \leq h_{s,2}, \\ \vdots & \vdots \\ \log a_m + b_m \log(h - h_{0,m}), & h_{s,m-1} \leq h. \end{cases} \quad (6)$$

396 In Eq. (6),  $Q_r$  is the estimated streamflow,  $h$  is measured gage height,  $h_{0,1}$  is the cease-to-flow  
 397 parameter of lowest power-law segment which corresponds to height of riverbed with respect to  
 398 datum,  $h_{s,k}$  is the upper bound of  $k^{th}$  power-law segment on  $h$  axis,  $h_{0,k}$  is the cease-to-flow  
 399 parameter of  $k^{th}$  segment,  $a_k$  and  $b_k$  are the multiplier and exponent parameters of the  
 400  $k^{th}$  segment, and  $m$  is the number of rating curve segments. Typically, several gage heights are  
 401 measured during a day which are then converted to streamflow using the rating curve. Equation  
 402 (6) corresponds to Mannings equation (Sturm, 2001) for flow in shallow and wide open channels  
 403 (with the assumption that hydraulic radius is approximately equal to depth; Le Coz et al., 2014)  
 404 and is a frequently used relationship in hydraulic modeling. Errors in gage height measurements  
 405 may be assumed negligible (Reitan and Overleir, 2009). Thus, uncertainties in estimated  
 406 streamflow are mainly due to errors in direct measurements of streamflow that are used to construct  
 407 the rating curve. In this study, the following model was used to quantify the uncertainties in  
 408 estimated streamflow

$$Q(h) = Q_r(h) + \epsilon_r, \quad (7)$$

409 where  $Q_r(h)$  is determined by Eq. (6),  $\epsilon_r$  is the random measurement error in observed streamflow  
 410 and  $Q(h)$  is the observed streamflow. Further, we assumed the  $\epsilon_r$ 's at different time-steps to be  
 411 distributed independently as skewed exponential power distribution (Fernandez and Steele, 1998).  
 412 Also,  $Q(h)$  was truncated at zero which makes the probability density of  $Q$  equal to

$$p_Q(Q) = \frac{2}{\gamma + \gamma^{-1}} \left\{ f_{\epsilon_r} \left( \frac{\epsilon_r}{\gamma} \right) \mathbf{I}_{[0,\infty)}(\epsilon_r) + f_{\epsilon_r}(\gamma \epsilon_r) \mathbf{I}_{(-\infty,0)}(\epsilon_r) \right\} \mathbf{I}_{[0,\infty)}(Q), \quad (8)$$

413 where  $\gamma \in (0, \infty)$  is the skew parameter,  $\mathbf{I}$  denotes the indicator function,  $\Phi(0|Q_r, \phi, \beta, \gamma)$  is the  
 414 probability that the value of untruncated  $Q$  is less than zero, and  $f_{\epsilon_r}$  is the power exponential  
 415 distribution with scale parameter  $\phi$  and shape parameter  $\beta \in (-1, 1]$ ,

$$f_{\epsilon_r}(\epsilon_r) = \Gamma^{-1} \left( 1 + \frac{2}{1 + \beta} \right) 2^{-\left(1 + \frac{2}{1 + \beta}\right)} \phi^{-1} \exp \left( -\frac{1}{2} \left| \frac{\epsilon_r}{\phi} \right|^{\frac{2}{1 + \beta}} \right). \quad (9)$$

416 The priors listed in Table 3 were used as weakly informative priors over parameters of the models  
 417  $Q_r$  and  $\epsilon_r$ , following Reitan and Overleir (2009). Strictly, uniform priors over the parameters of  
 418  $Q_r$  are not non-informative (Gupta et al., 2022). This difference, however, would have minimal  
 419 effect on our analysis as we are concerned only with the width of uncertainty bounds over  
 420 streamflow time series, not the probabilities assigned to different realizations of streamflow time  
 421 series. Further, we have not imposed any upper limit on the distribution of  $Q$ . Very low (practically  
 422 zero) probability will be assigned beyond a certain magnitude of  $Q$  (irrespective of the prior  
 423 distribution used) – the results obtained for the four SJRW stations confirm that absence of upper  
 424 limit does not have any effect on the obtained uncertainty bounds. Validity of the error model of  
 425 Eq. (8) was assessed a-posteriori via QQ plots.

426 The aleatoric assumption made in the analysis may not be valid during the peak events. It has been  
 427 shown using hydraulic modeling that uncertainty during peak events can be very high (Di  
 428 Baldassarre and Montanari, 2009). These uncertainties are epistemic in nature rather than aleatoric,  
 429 and, therefore, a formal statistical treatment of these uncertainties is difficult. To test how well the  
 430 QRF LOAs envelop the streamflow uncertainty due to these epistemic sources, we computed the  
 431 fraction of peaks enveloped by the QRF LOAs, if the true peaks were some multiple  $f$  of the  
 432 observed peaks, with  $f$  varying from 1.1 to 2. We refer to this analysis as the multiplier analysis  
 433 in this study. Only the peaks with flow values greater than 50-percentile were considered for this  
 434 analysis.

435 Table 3. List of priors over rating curve parameters

Parameter	Prior
$m$	$\mathcal{U}\{1,2,3\}$ – discrete uniform
$\log a_k$	$\mathcal{U}(0,8)$
$b_k$	$\mathcal{U}(0.5,3.5)$
$h_{0,1}$	$\mathcal{U}(-5, h_{min})$
$h_{s,k}$	$\mathcal{U}(h_{s,k-1}, h_{max})$
$h_{0,k}$	$\mathcal{U}(-5, h_{s,k-1})$
$h_{s,1}$	$\mathcal{U}(h_{0,1}, h_{max})$
$\phi$	$\mathcal{IG}(2,0.1)$
$\beta$	$\mathcal{U}(-1,1)$

$$\frac{\gamma}{\mathcal{U} = \text{Uniform}; \mathcal{G} = \text{Gamma}; \mathcal{IG} = \text{Inverse Gamma}}$$

$$\mathcal{G}(1/0.57, 0.57)$$

$$\text{Gamma distribution: } f(x) = \frac{1}{\Gamma(\alpha)\beta^\alpha} x^{\alpha-1} e^{-\frac{x}{\beta}}$$

436

437 The posterior distribution over parameters was computed using Delayed Rejection Adaptive  
 438 Metropolis (DRAM) algorithm (Haario et al., 2006) in an approximate Bayes setting (Nott et al.,  
 439 2012). The approximate Bayes computations facilitated faster convergence to a posterior  
 440 distribution. This method of rating curve analysis is same as that of Reitan and Overleir (2009)  
 441 except that they used a multiplicative error model instead of an additive error model. The  
 442 multiplicative error model was considered unsuitable in this case because of the large range of  
 443 streamflow values as opposed to that in Reitan and Overleir (2009) study: a multiplicative error  
 444 model would result in unrealistically high uncertainties at larger values of observed streamflow.  
 445 Additive error structure used in this study was found to be appropriate (by the way of QQ plot test)  
 446 in the examples considered in this study. Convergence to posterior distribution was confirmed  
 447 using R-diagnostic statistic ( $R_d$ ; Gelman and Rubin, 1992). Markov chains were assumed to  
 448 converge to posterior distribution if  $R_d$  converged to a value below 1.1 and never increased on  
 449 further simulations of the chains. The posterior distribution was further processed to remove the  
 450 parameter sets that yielded large deviations between observed and estimated streamflow: the  
 451 deviation between observed and estimated streamflow was measured using sum-of-square-errors.  
 452 The computed posterior distribution over parameters (of both  $Q_r$  and  $\epsilon_r$ ) was used to simulate  
 453 several streamflow time series that were assumed to represent random uncertainty in  
 454 measurements of streamflow, as obtained by the rating-curve method.

455

#### 456 *2.4 Uncertainty bound in areal average rainfall*

457 The uncertainty in areal average rainfall exists due to errors in rainfall measurements at a gauging  
 458 station and due to spatial interpolation. Errors in rainfall measurements at a gauging station are  
 459 difficult to obtain due to lack of a simple error model. The errors due to spatial interpolation are  
 460 likely to dominate the total error in areal average rainfall (e.g., Renard et al., 2011). Therefore, the  
 461 errors in rainfall measured at a gauging station are neglected in this study, and it is assumed that  
 462 the errors in areal average rainfall exist solely due to spatial variability of rainfall. Several different  
 463 models have been proposed to capture the spatial variation of rainfall such as cluster point Poisson  
 464 processes (Waymire and Gupta, 1981a, b, c), random cascades (Gupta and Waymire, 1993),  
 465 Kriging (Moulin et al., 2009), and conditional simulations (Renard et al., 2011). All these models  
 466 treat rainfall as a random field in space-time domain. But most of these models are typically based  
 467 on strict assumptions about the covariance of spatial error structure which are not justifiable in  
 468 practice. Even if the assumptions are approximately true, the rain gauge density is typically too  
 469 small to reliably estimate the parameters of the covariance function. This issue is further  
 470 complicated as the covariance structure may vary from event to event in unknown ways, depending  
 471 upon the type of event. Therefore, in this study, an empirical approach was used to get an estimate  
 472 of the uncertainty in areal average rainfall.

473 There were 6 rainfall gauging stations near the SJRW (locations on these stations are shown in  
 474 Figure B1) at which daily timescale data were available. Typically, data from the available rain  
 475 gauges are used to compute a single areal average rainfall time series using the Thiessen polygon  
 476 interpolation method. In this study, all the  $63 = (2^6 - 1)$  different combination of the 6 rain

477 gauges were used to produce 63 realizations of areal average rainfall using the Thiessen polygon  
478 method. These 63 realizations represent an estimate of uncertainty in areal average rainfall.

479

## 480 2.5 Uncertainty bounds using runoff ratio method

481 The QRF method does not allow one to incorporate a hydrologists' knowledge about a watershed  
482 to construct the measurement uncertainty bounds. One method that allows incorporation of such  
483 knowledge was proposed by Beven (2019) using runoff ratios of observed rainfall-runoff events.  
484 In this method, only the observed rainfall-runoff data (along with evaporation data) of the  
485 watershed in question are used to create LOAs. This method was used to derive LOA estimates  
486 that were then compared to the LOAs estimated by the QRF algorithm.

487 In the first step, the observed rainfall-runoff data were separated into different rainfall-runoff  
488 events. This kind of hydrograph separation requires estimation of the recession curve. To this end,  
489 the master recession curve (MRC) technique was used (Lamb and Beven, 1997) – MRC is a  
490 characteristic recession curve of the watershed (Tallaksen, 1995). Once an MRC is defined, the  
491 streamflow time series can be divided into different rainfall-runoff events. In this study, a rainfall  
492 value below  $1 \text{ mm day}^{-1}$  was considered negligible, and a new rainfall event was assumed to start  
493 if the rainfall was negligible for more than 7 consecutive days. For example, a new rainfall event  
494 started at time-step  $t_n$  if the rainfall values at the time-steps  $t_{n-1}, \dots,$  and  $t_{n-7}$  were less than  
495  $1 \text{ mm day}^{-1}$ . The streamflow hydrograph corresponding to each rainfall event was assumed to  
496 start at the beginning of the rainfall event and end just before the start of next rainfall period. Next,  
497 MRC was appropriately appended at the end of the streamflow hydrograph for each rainfall-runoff  
498 event. The number of rainfall-runoff events, thus obtained for four of the stations in SJRW, are  
499 listed in Table 4.

500 In the second step, the runoff ratio of each event was computed as the ratio of the total volume of  
501 event streamflow to the total volume of event rainfall, where 'event streamflow' refers to  
502 streamflow time series obtained after appending the MRC. This resulted in an ensemble of runoff  
503 ratios. In the third step, uncertainty bounds over measurement errors were computed over each of  
504 the rainfall-runoff events in an iterative manner. To construct the bounds over the  $i^{th}$  event, the  
505 events in the ensemble similar to the  $i^{th}$  event were identified based on antecedent moisture  
506 condition and total volume of rainfall during the event. As an estimate of the antecedent moisture  
507 conditions, initial streamflow of the event was used. Thus, the events that were closest to the  $i^{th}$   
508 event were identified by using the Mahalanobis distance between the events using these two  
509 variables (this is the k-nearest neighbor approach used by Beven, 2019). Appropriate value of the  
510 Mahalanobis distance to define the closeness of two events is a subjective decision. In this study,  
511 we first computed the Mahalanobis distance of the  $i^{th}$  event from rest of the events, and, then  
512 normalized the distance values to lie between 0 and 1. Now, events similar to the  $i^{th}$  event may be  
513 defined as the events that are  $d_{M,N}$  distance away from the  $i^{th}$  event, where  $d_{M,N}$  denotes  
514 Mahalanobis distance. Several values of  $d_{M,N}$  were used to analyze the impact of this threshold on  
515 uncertainty bound. After the completion of the third step, one obtains runoff ratios of the  $i^{th}$  event  
516 and those of other  $N_i$  events that are similar to the  $i^{th}$  event. In addition to the k-nearest neighbor  
517 approach, we also used decision tree approach to group the similar events, again based on  
518 antecedent moisture condition and total rainfall volume. In what follows, the abbreviations RR-

519 KNN and RR-QRF will be used to refer to runoff ratio method applied using k-nearest neighbor  
520 method and QRF method, respectively.

521 In the fourth step, the streamflow time series of the  $i^{th}$  event was divided by its runoff ratio  $C_i$ ,  
522 thus yielding a zero-loss streamflow time series of the  $i^{th}$  event that would have been observed if  
523 the runoff ratio of the  $i^{th}$  event was equal to 1. The zero-loss streamflow time series was then  
524 multiplied by the largest and smallest runoff ratios to obtain time series upper and lower bound of  
525 LOA. In RR-KNN method, the largest and smallest runoff ratios were identified among the  $N_i$   
526 runoff ratios of the events similar to the  $i^{th}$  event. In RR-QRF approach, the largest and smallest  
527 runoff ratios were the 100<sup>th</sup> and 0<sup>th</sup> percentiles in the leaf node to which the  $i^{th}$  event belonged.  
528 RR-QRF approach is more objective than the RR-KNN approach since the value of  $d_{M,N}$  needs to  
529 be specified subjectively in the later. However, specification of appropriate percentiles in RR-QRF  
530 incurs some subjectivity.

531 Table 4. Number of rainfall-runoff events for each of the USGS stations in the SJRW

<b>USGS station</b>	<b>Number of rainfall- runoff events</b>
04180500	138
04180000	148
04179520	139
04178000	146

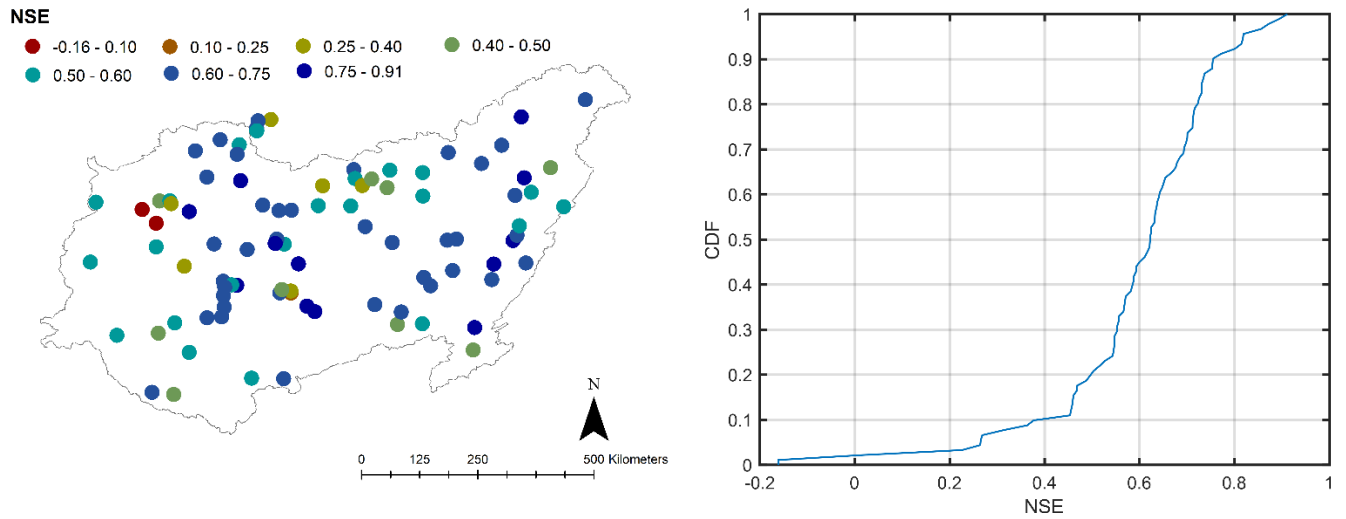
532

### 533 3. Experiments with rainfall-runoff data

#### 534 3.1 Can decision trees (DTs) account for measurement uncertainty due to errors in rainfall and 535 streamflow measurements?

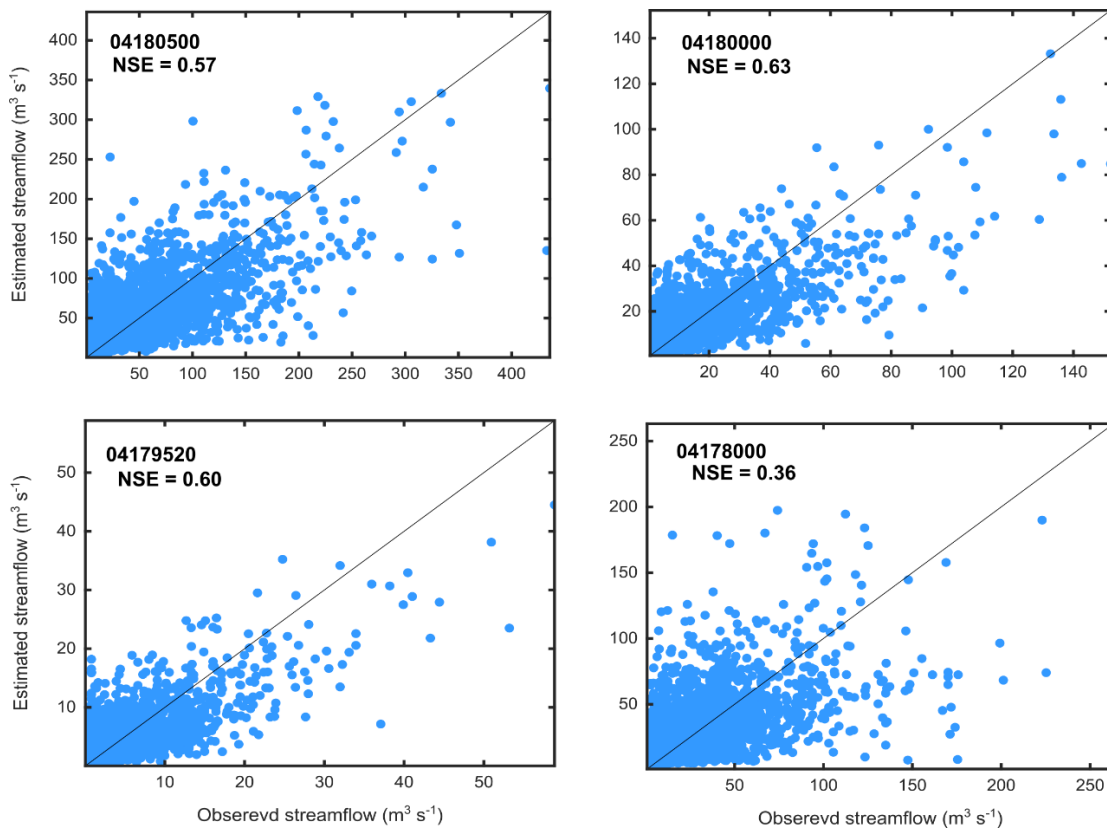
536 Figure 3 shows the NSE values obtained by the RF ungauged model for the watersheds contained  
537 in the test set. NSE was greater than 0.60 for 55% of the watersheds and was greater than 0.5 for  
538 80% of the test watersheds. There were some systematic patterns in the spatial distribution of NSE  
539 values. NSEs were typically higher in the eastern part of the basin than those in the western part.  
540 Most watersheds in the eastern ORB had NSEs greater than 0.5. For about 20% of all the test  
541 watersheds, the NSE was less than 0.5. It is likely that the RF algorithm could not identify the  
542 rainfall-runoff relationship in these watersheds, possibly because the hydrological behavior of  
543 these watersheds is not represented in the data. Overall, the performance of the RF model was  
544 deemed acceptable for majority of the watersheds for which NSE was greater than 0.50. It captured  
545 the rainfall-runoff dynamics in the sense that its response to input rainfall is hydrologically  
546 consistent. The term ‘hydrologically consistent’ is used to refer to an expected behavior of  
547 hydrologic models: increasing streamflow with increasing rainfall under similar antecedent  
548 conditions. One question is if QRF model can be used to construct LOAs in a watershed where the  
549 NSE is low. We note that low NSE value can also be due to errors in streamflow or rainfall data.  
550 But still the LOAs obtained for these watersheds may not be reliably used for model inference.  
551 Figure 4 shows the observed and predicted streamflow for the four stations located in SJRW. NSE  
552 was close to 0.6 for the three of the stations but was poor (=0.36) for station 04178000. These  
553 values seem adequate for constructing measurement uncertainty bounds except for the station  
554 04178000.





555 Figure 3. (a) Spatial distribution of NSE values for the test set including ORB and SJRW station,  
 556 and (b) cumulative distribution function (CDF) of the test NSE values. These NSE values were  
 557 derived from ungauged model.

558



559 Figure 4. Observed vs. estimated streamflows at four stations in St. Joseph River Watershed  
 560 (SJRW). The estimated streamflow values were derived from ungauged model.

561

562 *3.2 Limits-of-Acceptability (LOA) constructed by the QRF models*

563 Figure 5 shows the LOAs obtained by the QRF models trained under the first two scenarios  
564 (gauged-single and gauged) along with the uncertainty bounds obtained by the rating-curve  
565 analysis. Since rating curve analysis yields uncertainty due to errors in streamflow measurements  
566 only, LOAs obtained by QRF should envelop the uncertainty bound obtained by rating curve  
567 analysis as shown in Figure 5. A similar observation was made for the majority of the study period  
568 (not shown). Among the different QRF models (QRF-gauged-all, QRF-gauged-20, QRF-gauged-  
569 4, QRF-single), the LOAs obtained by the QRF-gauged models were widest and the LOAs  
570 obtained by the QRF-gauged-20 and QRF-gauged-4 models were typically close to each other.  
571 The QRF-single model yields very narrow LOAs at the two peaks shown (at time-steps 410 and  
572 438). These two peaks are among the highest flow values observed in these watersheds implying  
573 that more data are required to construct reliable LOAs for these peaks. This illustrates the practical  
574 difficulty in constructing LOAs and highlights the need to allow for outliers when LOAs are used  
575 for model inference. There would not be enough data to estimate LOAs for events with return  
576 period greater than 2 to 10 years in many instances. The LOAs obtained by the three QRF-gauged  
577 models (QRF-gauged-all, QRF-gauged-20, QRF-gauged-4) were very similar except at a few time  
578 steps. As mentioned above, the 4 and 20 most similar watersheds to train the QRF model were  
579 identified using some watershed static attributes. These static attributes are already used by the  
580 QRF method to partition the data into leaf nodes, which explains the similarity of LOAs obtained  
581 by the three gauged models.

582 The uncertainty bound obtained by rating curve analysis was significantly narrower at most of the  
583 time-steps indicating that errors in rainfall measurements contribute more to measurement  
584 uncertainty than do the errors in streamflow measurements. But the streamflow uncertainty bounds  
585 shown in Figure 5 were obtained by making aleatoric assumptions. The peak streamflow values  
586 may contain larger uncertainties. Figure 6 shows the fraction of peaks enveloped by upper bounds  
587 of LOAs if the observed peak magnitude were multiplied by a factor  $f$ . As the multiplier  $f$   
588 increases, the fraction of peaks enveloped by the QRF uncertainty bound decreases. This decrease,  
589 however, occurs at different rates for the three models. Interestingly, the fractions of multiplied  
590 peaks were larger for the gauged-single model than the ones obtained by the gauged-all model.  
591 This is likely to be because of timing errors in precipitation data as discussed below. The typical  
592 errors in peak streamflow have been reported to be 20-40% (Di Baldassarre and Montanari, 2009);  
593 Figure 6 shows that more than 55% of the peaks were enveloped in these ranges of errors by all  
594 the three models. Even for 100% errors, more than 30% of the peaks are enveloped by the QRF  
595 bounds across the three models.

596 One of the characteristics of the uncertainty bound obtained by the QRF method (Figure 5) is that  
597 it is very wide at the time-steps corresponding to streamflow peaks and narrow at the time-steps  
598 where streamflow is small. Although not shown here, this pattern was visible throughout the study  
599 period. Figure 7 shows the standard deviations of streamflow obtained by QRF method plotted  
600 against streamflow. The standard deviation increases as streamflow value increases in keeping  
601 with how rainfall uncertainty typically propagates to streamflow uncertainty (Moulin et al., 2009;  
602 Renard et al., 2011). These observations suggest that QRF is able to account for the effect of  
603 uncertainty due to rainfall and streamflow measurement errors.

604 One seeming discrepancy to the pattern discussed above is the wide LOA obtained by the QRF-  
605 gauged method between time-steps 410 and 420 even when the streamflow time series is in  
606 recession phase (Figure 5) – this is especially the case for the stations 04180500 and 04178000.  
607 Data show that some rain did fall over the watershed at these time-steps (Figure 5), and this rain

608 event was similar in magnitude to the rain event that generated the streamflow peak at time-step  
609 424. One possibility is that this rain event did not result in streamflow due to spatial location of  
610 the event (rain event might be far from the watershed outlet). The second possibility is that the  
611 rainfall measurement at the gauging station is erroneous. Third source of error is the unknown true  
612 intensity of the rainfall. The observed rainfall data are at daily timescale; two events with same  
613 intensity at the daily timescale may have very different intensities at sub-daily timescales which  
614 will result in different hydrographs. These are examples of epistemic errors, and the exact reason  
615 for these errors is difficult to know. In fact, we do not even know whether the measurement is  
616 actually erroneous. A good hydrologic model forced with this rain event and uninformed by *true*  
617 spatial distribution and true intensity of rainfall will still generate a streamflow event (if the  
618 antecedent conditions allow). It would be unwise to reject this model if these errors indeed exist.  
619 This illustrates how QRF can account for epistemic errors. Similarly, at time-step 450, a wide  
620 LOA was obtained by the QRF method for three of the stations whereas streamflow time series is  
621 in recession phase. Again, a rainfall event was observed at this time-step which apparently did not  
622 result in a streamflow peak, and the same arguments apply.

623 In some of the events, timing errors between observed peak and QRF simulated peak were  
624 observed – these timing errors were mostly present in the LOAs created by the QRF-gauged model.  
625 An example of such timing errors may be seen at time-step 438 in Figure 5. These timing errors  
626 occurred for less than 20 events per watershed (see also Figure 11 where LOAs for a few other  
627 time-steps are also shown). For the five peak events shown in Figure 5, timing error occurs only  
628 for one event for the three stations 04180500, 04180000, 04179520. Out of the two major peaks  
629 at time-steps 410 and 438, timing errors are not present at time-step 410 for these three stations.  
630 Similarly, for station 04179520, the timing errors are not present even at time-step 438. For two  
631 of the stations (04180500 and 04180000), timing errors at time-step 438 are present.

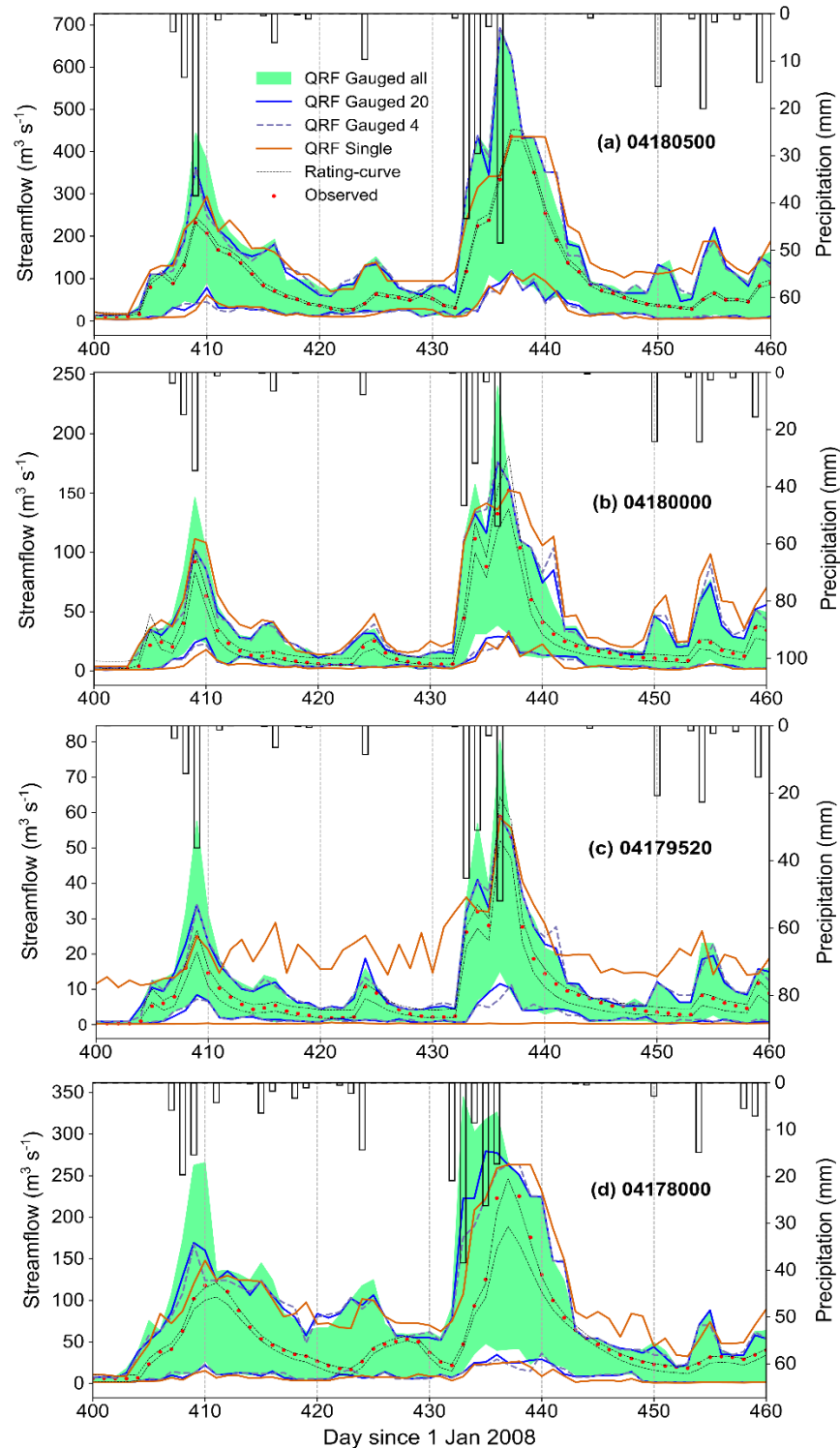
632 There seem to be two possibilities behind these timing errors: (1) disinformation introduced by the  
633 data from other watersheds, or (2) timing errors in rainfall data. For the stations 04180500 and  
634 04180000, there is zero lag between rainfall and QRF obtained streamflow peak at time-step 410.  
635 Meanwhile at time-step 438, a lag of 1-2 days between rainfall and streamflow peak is observed.  
636 Further, the rainfall event at time-step 438 is more intense (at daily timescale) and one would  
637 expect a smaller lag between rainfall and streamflow peaks for this event compared to the lag  
638 observed for the event at time-step 410. Therefore, it seems more likely that the computed areal  
639 average rainfall has timing errors for this event. We note that it is also possible that the sub-daily  
640 timescale intensity of the event at time-step 438 was low which would justify the delay in peak.  
641 This is again an example of epistemic uncertainty.

642 The same arguments apply for the timing errors observed at the station 04178000, especially at  
643 time-step 424 where the lag between computed areal rainfall peak and observed streamflow is 3  
644 days. The timing errors at the station 04178000 were more frequent which is partly the reason for  
645 poor validation NSE value at this station (Figure 4). It is worth noting that the timing errors  
646 between LOAs constructed by QRF-single model and streamflow were typically absent. It is  
647 possible that the model has compensated for timing errors in precipitation.

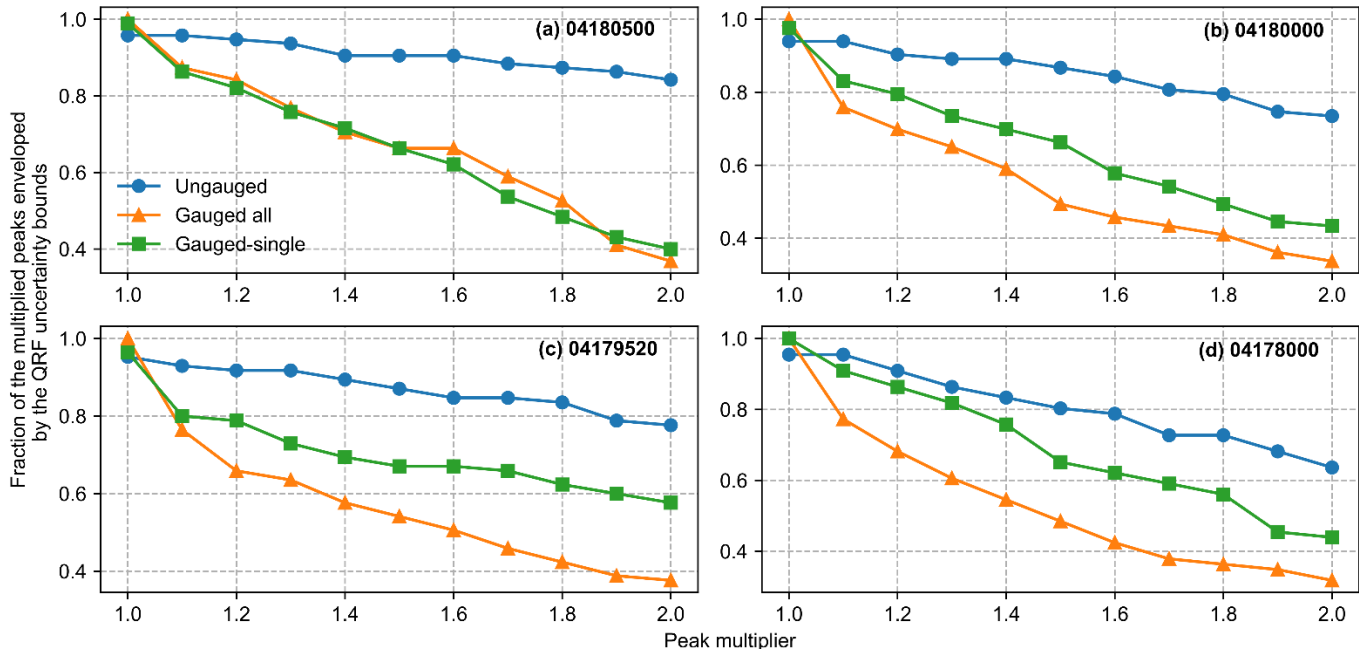
648 Potential for the timing errors in rainfall around time-step 438 is also illustrated in Figure 8 which  
649 shows all the different realization of the areal average rainfall. For the majority of the realizations,  
650 the second precipitation peak occurs at time-step 436 while for a few realizations the second peak  
651 occurs at time-step 435. These realizations were constructed using six gauging stations which are

652 located outside but near the SJRW watershed (Figure B1). If data from more stations were  
653 available, some of the realization might have very well shown the second peak at the time-step  
654 437.

655 It is worth noting that the information about timing error may not be revealed by QRF-single model  
656 as it will learn this as a behavior of the watershed. Thus, this analysis illustrates the usefulness of  
657 data from different watersheds in constructing LOAs. This also illustrates how the LOAs  
658 constructed using decision trees may potentially capture the effect of timing errors. However, it is  
659 also possible that the timing errors between the observed and QRF (gauged model) simulated peaks  
660 occur because of disinformation introduced by data from other watersheds. Therefore, it seems  
661 more prudent to construct different LOAs using different kinds of data and use a combination of  
662 these LOAs for model inference.



663 Figure 5. LOAs obtained by quantile random forest (QRF) in different gauged scenarios: using  
 664 all the training watersheds (green band), 20 most similar watershed including the four SJRW  
 665 watersheds (blue lines), 4 SJRW watersheds (blue-dash lines), and gauged single model (orange-  
 666 solid lines). Uncertainty bounds obtained by rating curve analysis (black-dash), and observed  
 667 streamflow (red dots), along with precipitation are also shown.



668 Figure 6. Fraction of the peaks enveloped by the QRF uncertainty bounds if the observed peaks  
 669 were 10-100% greater.

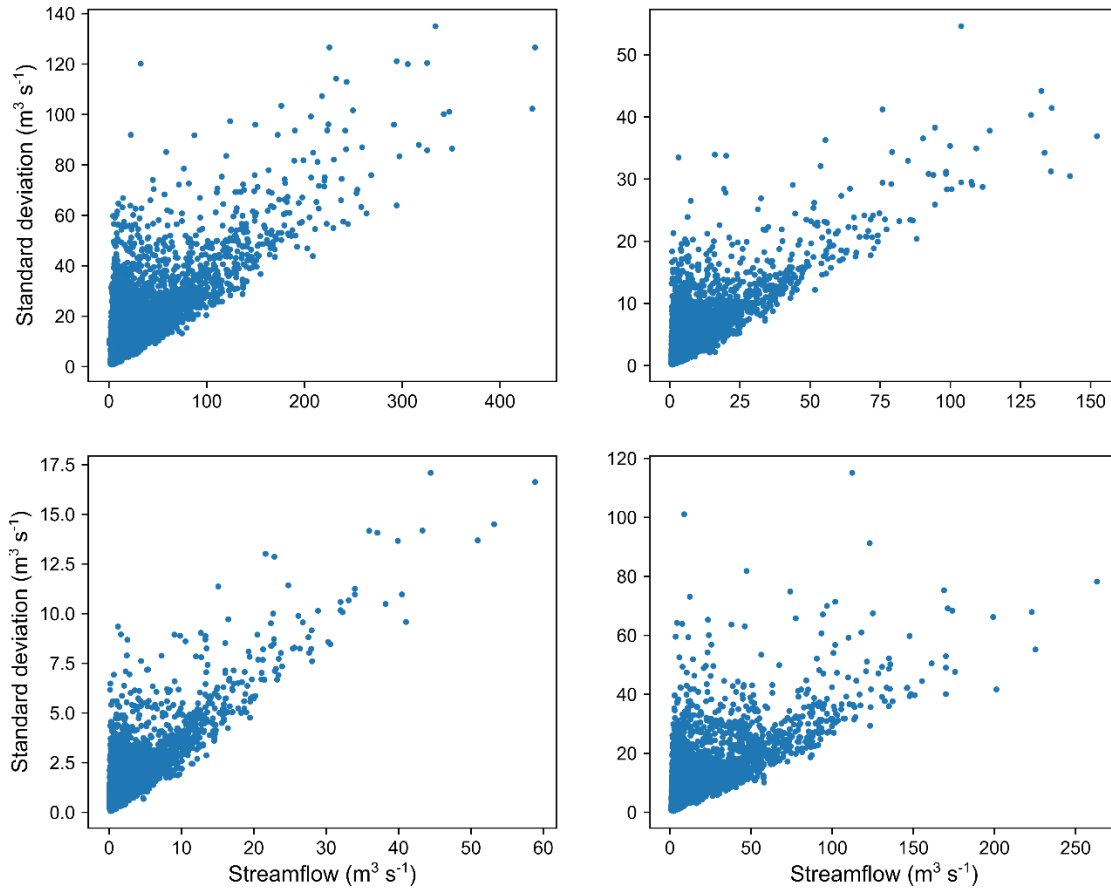
670

671

Table 4. Fraction of observations enveloped by the QRF LOAs

	QRF ungauged	QRF gauged	QRF gauged-single
04180500	0.97	1.00	0.99
04180000	0.97	1.00	0.99
04179520	0.94	1.00	0.99
04178000	0.96	1.00	0.99

672



673 Figure 7. Standard deviation of streamflow time series obtained by RF method plotted against  
 674 observed streamflow data. The standard deviation increases with increase in streamflow value.

675

676 Figure 9 shows the  $CV_R$  (coefficient of variation) of areal average rainfall obtained by using the  
 677 empirical approach described above. The  $CV_R$  values decrease as areal average rainfall increases,  
 678 at all the stations. At first one may attribute this behavior to standard deviation of rainfall being  
 679 constant irrespective of the mean rainfall value. However, it was observed that standard deviation  
 680 of areal average rainfall increases with increasing mean rainfall values (now shown) similar to the  
 681 standard deviation of streamflow. The  $CV$  values of excess rainfall, obtained by SCS-CN method,  
 682 also follow the same pattern as areal average rainfall. But the  $CV$ s corresponding to excess rainfall  
 683 were typically higher than the  $CV$ s corresponding to areal average rainfall. The difference between  
 684 excess and areal average rainfall  $CV$ s become smaller for higher values of areal average rainfall.  
 685 Many of the small non-zero areal average rainfall values produce no excess rainfall; increased  
 686 number of zeros in excess rainfall increases the  $CV$ .

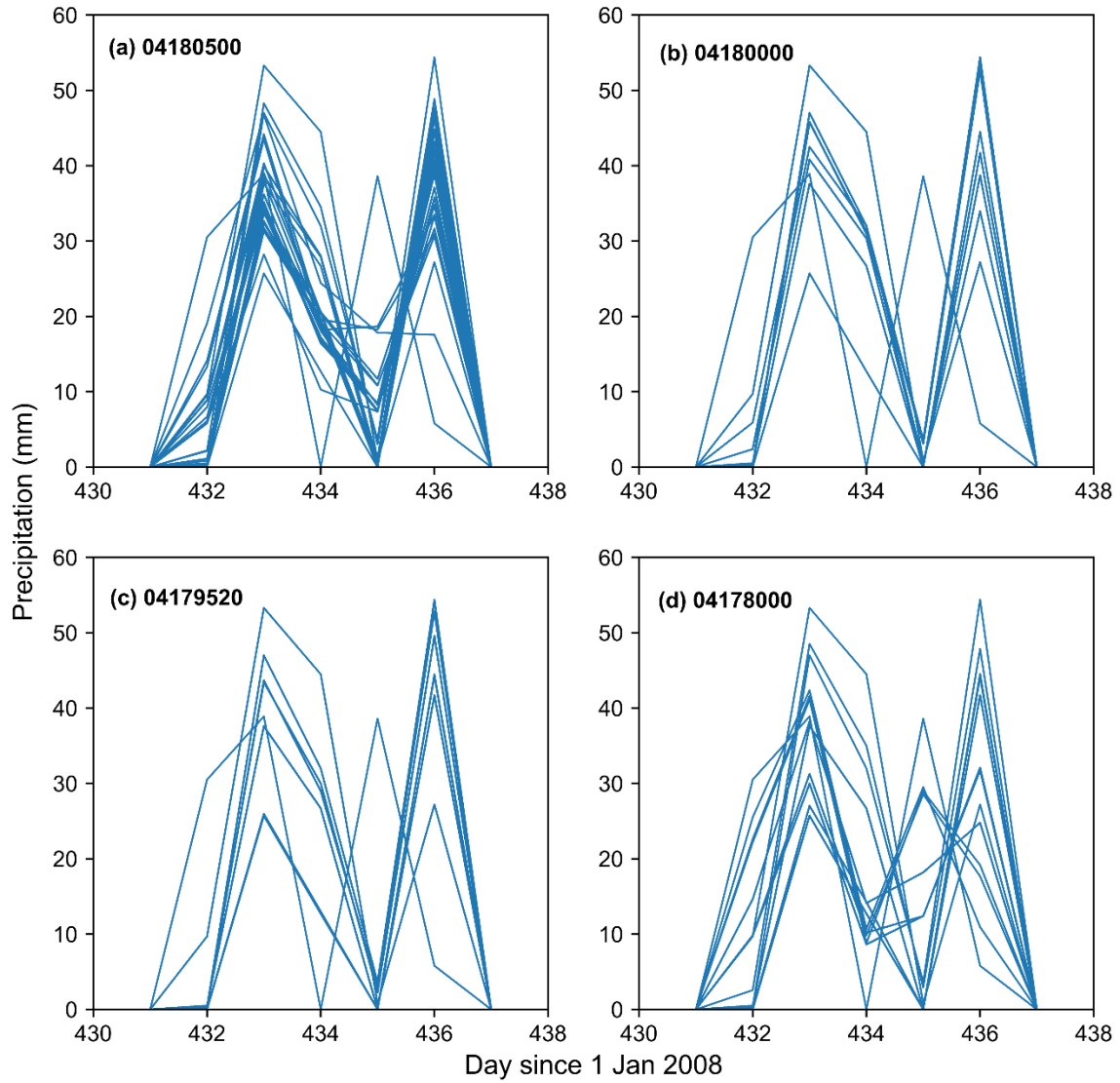
687 Figure 9 shows that variation of  $CV_Q$  with streamflow follows the same pattern as that of variation  
 688 of  $CV_R$  with mean areal average rainfall;  $CV_Q$  decreases as mean streamflow increases. For all the  
 689 four stations, the magnitudes of  $CV$ s are of similar order for the areal average rainfall and  
 690 streamflow time series. Another pattern in  $CV_R$  plots is that there is a larger (smaller) scatter in  
 691 these values when mean rainfall is small (large). The same pattern can be seen in streamflow values

692 also. The rainfall time series is transformed non-linearly through a watershed to yield streamflow.  
693 The same rainfall event can result in very different streamflow hydrograph depending upon the  
694 spatial distribution of rain within the watershed and antecedent moisture conditions. Thus, for a  
695 given rainfall magnitude, many different values of streamflow are possible which explains the  
696 larger scatter in  $CV_Q$ . Figure 9 indicates that the statistical structure of RF uncertainty bound  
697 reflects the effect of rainfall uncertainty. Overall, these results combined with the results discussed  
698 above indicate that the DTs could account for the effect of uncertainty due to errors in rainfall and  
699 streamflow measurements.

700 Further, it can be argued that any model with heteroscedastic error structure would result in  
701 uncertainty bounds as shown in Figure 5. The QRF method does not enforce heteroscedastic error  
702 structure, rather this error structure was identified by the algorithm from the data. The experiments  
703 with synthetic data showed (results not shown) that if the errors are homoscedastic, QRF produces  
704 homoscedastic error structure, and if the errors are heteroscedastic, QRF produces a  
705 heteroscedastic error structure. We emphasize that LOAs shown in Figure 5 do not represent  
706 measurement uncertainty only – it is likely that structural errors of QRF model are also  
707 contributing to these bounds.

708

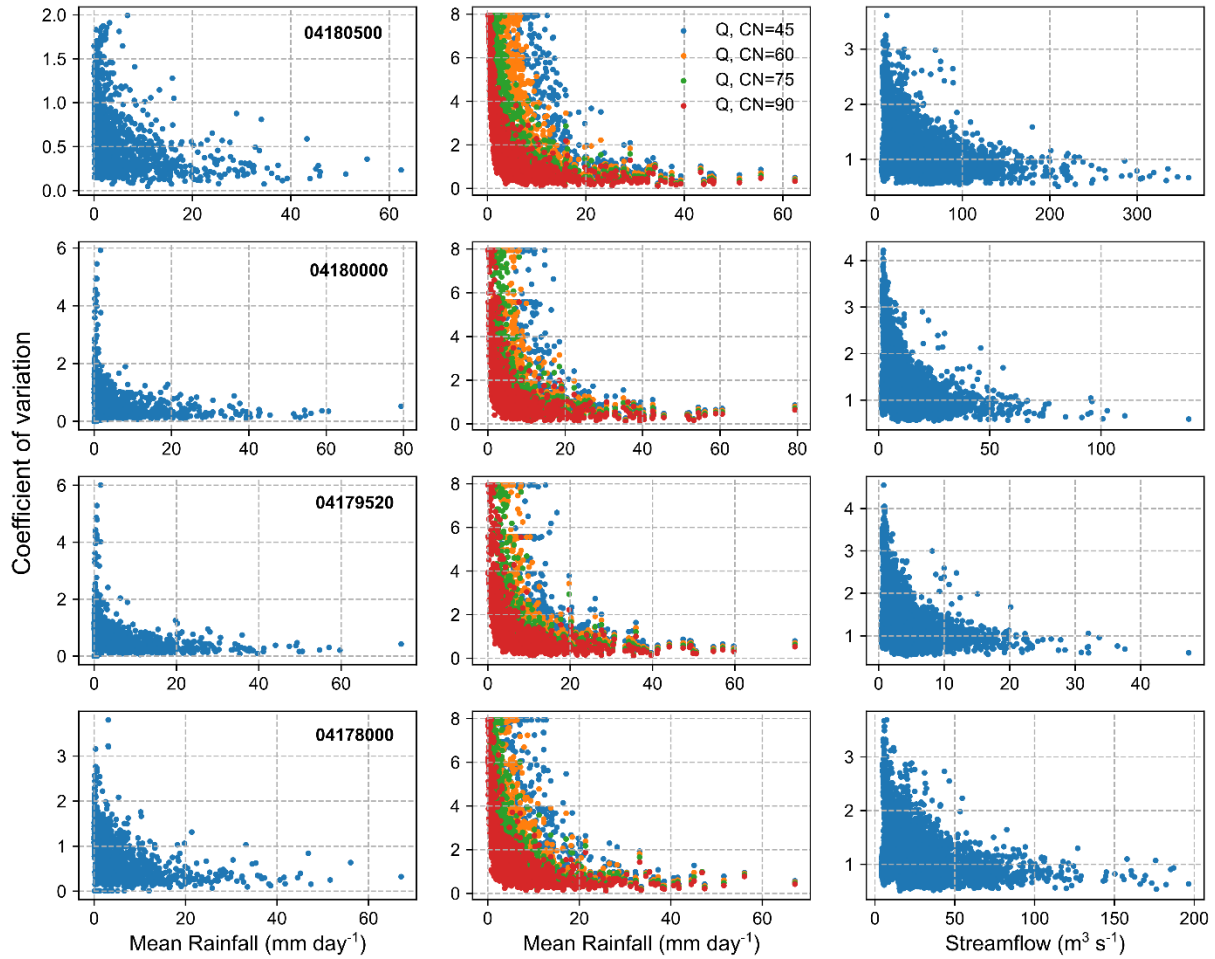




709

Figure 8. Different realizations of areal average precipitation

710



711 Figure 9. Coefficients of variation (CV) of areal average rainfall (left), excess rainfall for  
 712 different values of  $CN$  (middle), and the CV of streamflow obtained by RF in ungauged scenario  
 713 (right). In the legend,  $Q$  refers to excess rainfall obtained by using SCS-CN method for different  
 714 value of the parameter  $CN$ . Each row refers to one basin.

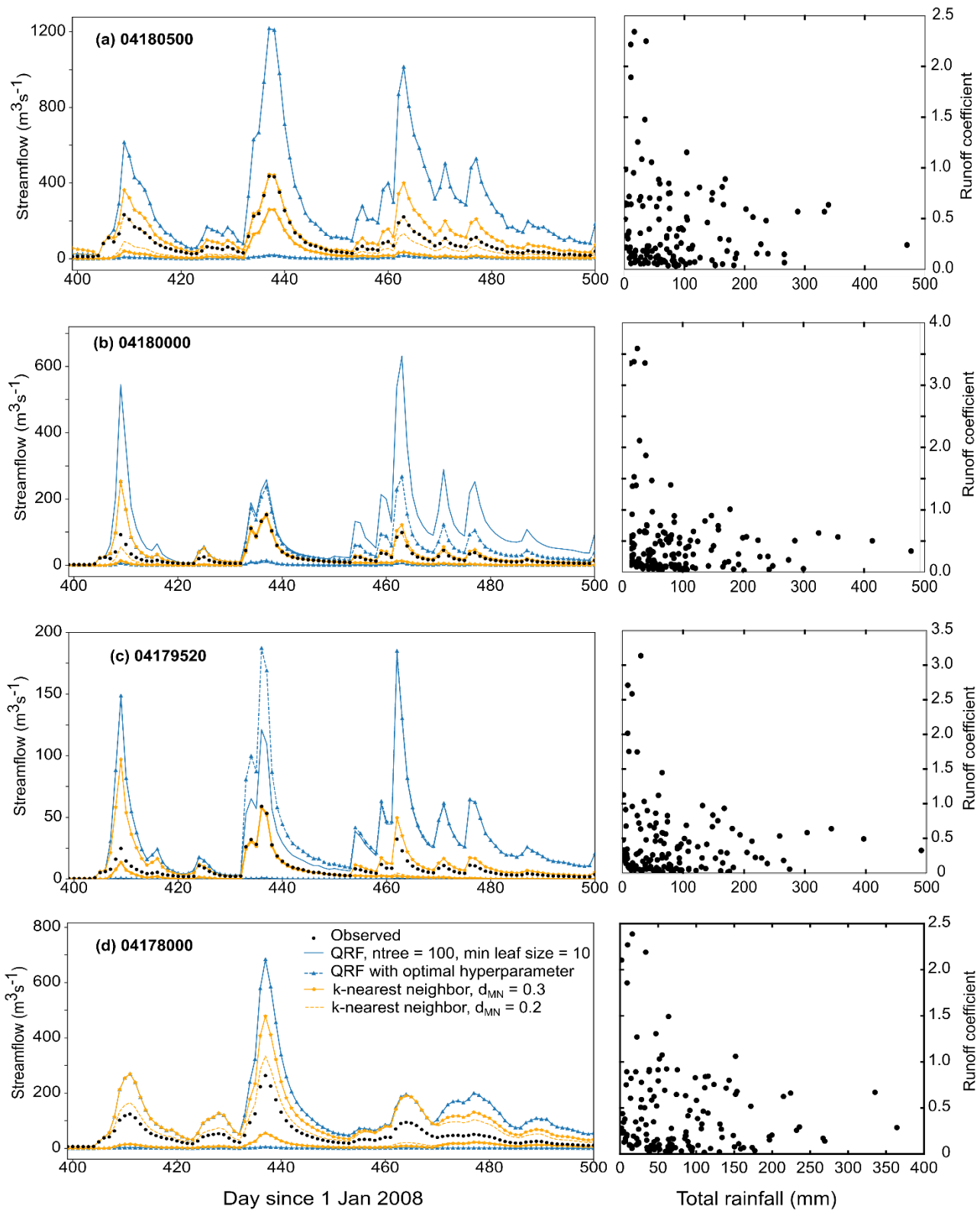
715

716 3.4 How does QRF LOAs compare to the LOAs obtained by the runoff ratio method?

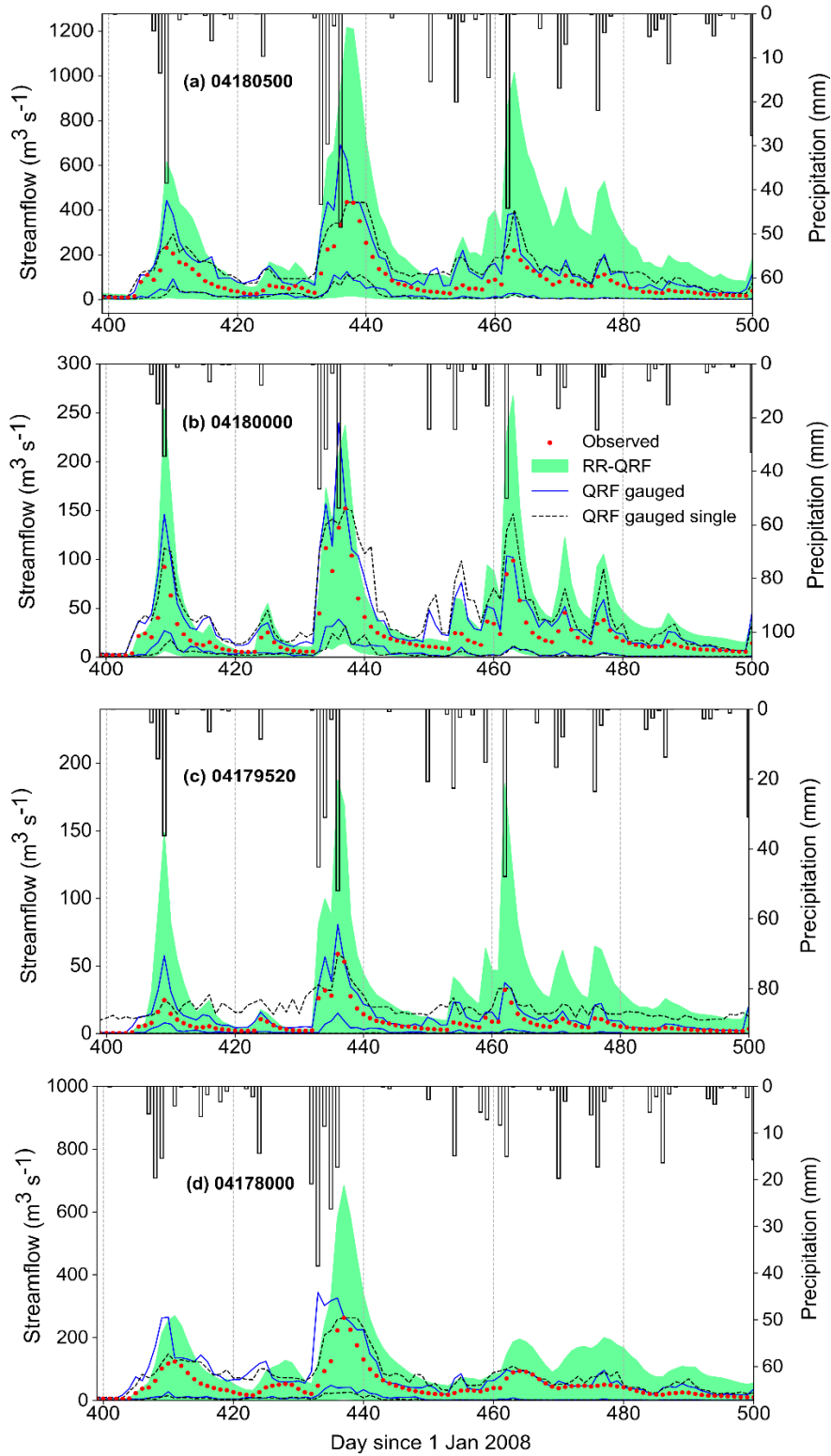
717 Figure 10 shows the uncertainty bounds obtained by runoff ratio method, along with the ensemble  
718 of runoff ratios at four of the gauging stations in SJRW. Ideally, the runoff ratios should lie  
719 between 0 and 1. The errors in rainfall and streamflow measurements, and inexactness of  
720 hydrograph separation method, however, may result in values of runoff ratios greater than one  
721 (Beven and Westerberg, 2011). Indeed, a few rainfall-runoff events had runoff ratio values greater  
722 than 2 which are likely to have occurred due to significant biases in rainfall measurements. These  
723 periods can be referred to as disinformative periods (Beven and Westerberg, 2011) which should  
724 not be used for parameter estimation and uncertainty analysis. In this study, however, these events  
725 were kept for further analysis as the final aim is to compare the bounds obtained by different  
726 methods. It may be noted that QRF will not recognize such disinformative periods, which  
727 emphasizes the importance of developing methods of uncertainty quantification based on  
728 hydrological reasoning. The QRF method, however, will yield appropriate uncertainty bound for  
729 these events making it unlikely that a good model will be rejected by using the LOAs obtained by  
730 the QRF algorithm even if it includes disinformative periods. For example, if a rainfall event has  
731 large negative bias, QRF will identify this event as similar to other events with small rainfall and  
732 the LOAs for this event will span a large range of streamflow values.

733  
734 Figure 10 shows the LOAs obtained by using the runoff ratio method where similar events were  
735 selected using KNN method (with two different distance thresholds  $d_{M,N} = 0.2$  and  $0.3$ ) and by  
736 using QRF method. One expects the LOAs to envelop all the observations and the uncertainty  
737 bounds to become wider as the value of  $d_{M,N}$  increases. This is indeed observed in Figure 10 with  
738 the following special case: the observations coincide with the upper uncertainty bound at a few  
739 time-steps for small  $d_{M,N}$  values. These cases occur because of the small number of rainfall-runoff  
740 events available at a station and even smaller number of similar rainfall-runoff events; this  
741 prohibits the construction of meaningful uncertainty bounds. LOAs obtained by RR-QRF method  
742 typically yield wider uncertainty bounds than the RR-KNN method which is partly a consequence  
743 of using 0% and 100% percentile values of data in the leaf node for defining these bounds (see  
744 Section 2.5).

745  
746 QRF-gauged algorithm uses information across several watersheds to construct LOAs, while  
747 runoff ratio method uses information available at only one gauging station to construct LOAs.  
748 Therefore, one can expect that the former will yield tighter uncertainty bounds compared to runoff  
749 ratio method. It is true for at least a few time-steps at four of the gauging stations in the SJRW for  
750 which this analysis was carried out (Figure 11). But at other times-steps, e.g., between 400 and  
751 420, the QRF uncertainty bound was wider. We note that the wide LOAs obtained by the RR-QRF  
752 method are partly a result of using 0 and 100% values of the data in the leaf node. There is one  
753 general similarity between the LOAs obtained by QRF and runoff ratio method: the width of both  
754 LOAs increase or decrease synchronously in time (except a few timing errors, see above for a  
755 discussion of this issue). This gives us further confidence that the LOAs obtained by QRF is able  
756 to capture general patterns of measurement uncertainty. If the patterns of LOAs obtained by QRF  
757 and runoff ratio method were significantly different, that would have disproved the usefulness of  
758 QRF in constructing LOAs. Therefore, we conclude that the proposed hypothesis cannot be  
759 rejected based on the analysis carried out in this study.



760 Figure 10. LOAs obtained by runoff ratio method (left) and runoff ratios plotted against total  
 761 rainfall of the each of the rainfall-runoff events (right).

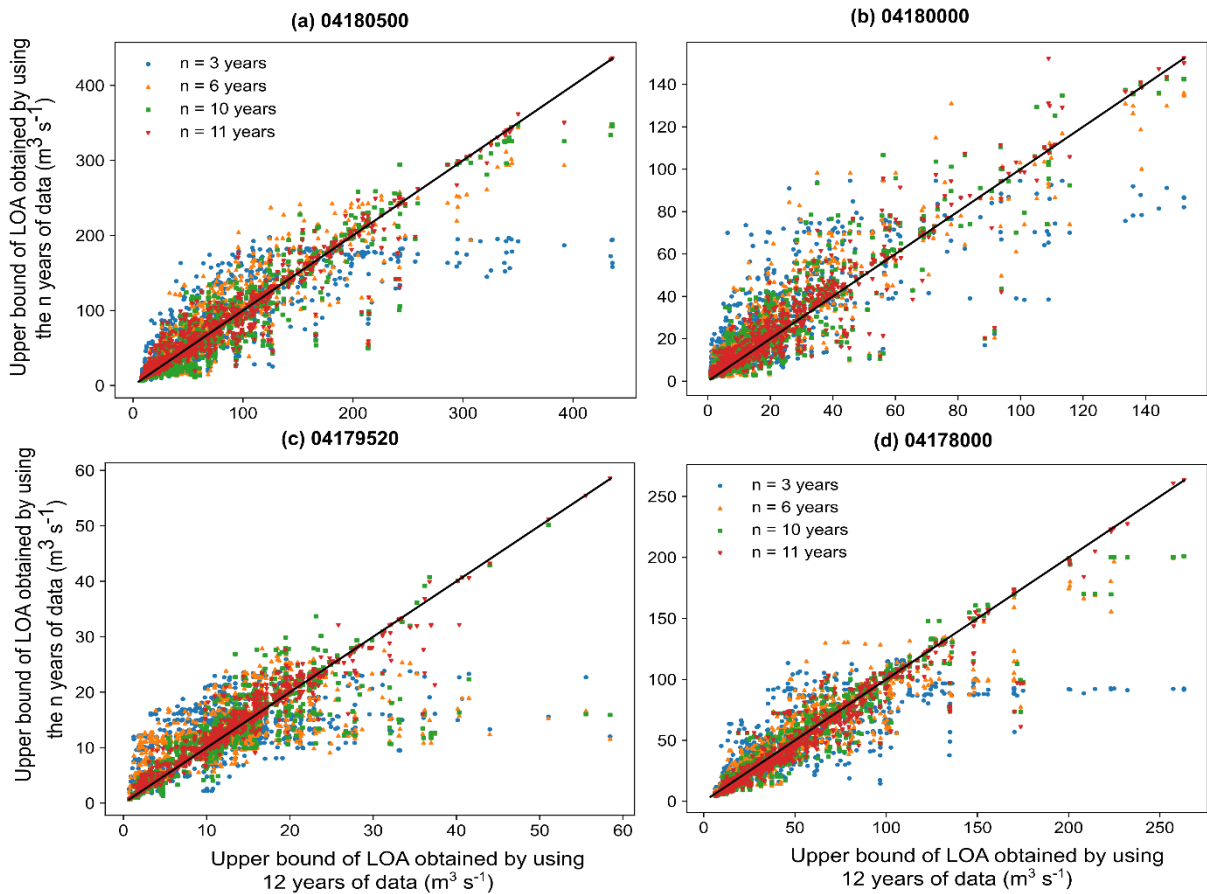


762 Figure 11. LOAs obtained by QRF-gauged-all (blue -solid), QRF-single (black-dash), and RR-  
 763 QRF (green band) methods along with observed precipitation and streamflow

764

765 3.4 Convergence of LOAs obtained by QRF algorithm

766 To test the convergence properties of QRF estimated LOAs with increasing length of data, several  
767 QRF models were developed using different lengths of training data. In these experiments, data  
768 from only that watershed where LOAs are to be constructed were used, i.e., gauged-single models  
769 were developed. For each of the four test watersheds, 12 different gauged-single models were  
770 developed using 1,2, ...,12 years of data. Figure 12 shows the 97.5<sup>th</sup> percentiles of LOAs thus  
771 obtained using different amounts of data. For three stations (04180500, 04180000, and 04178000),  
772 LOA estimates at high flow time-steps started to converge when more than three years of data  
773 were used, but there were a few high flow time-steps where LOAs did not converge. At station  
774 04179520, the convergence of LOAs seems to be much slower than the convergence at other  
775 stations. For low flows also, LOAs appear to be converging but more data are required to achieve  
776 the final bounds.



777 Figure 12: Convergence properties of LOAs obtained by the QRF algorithm.

778

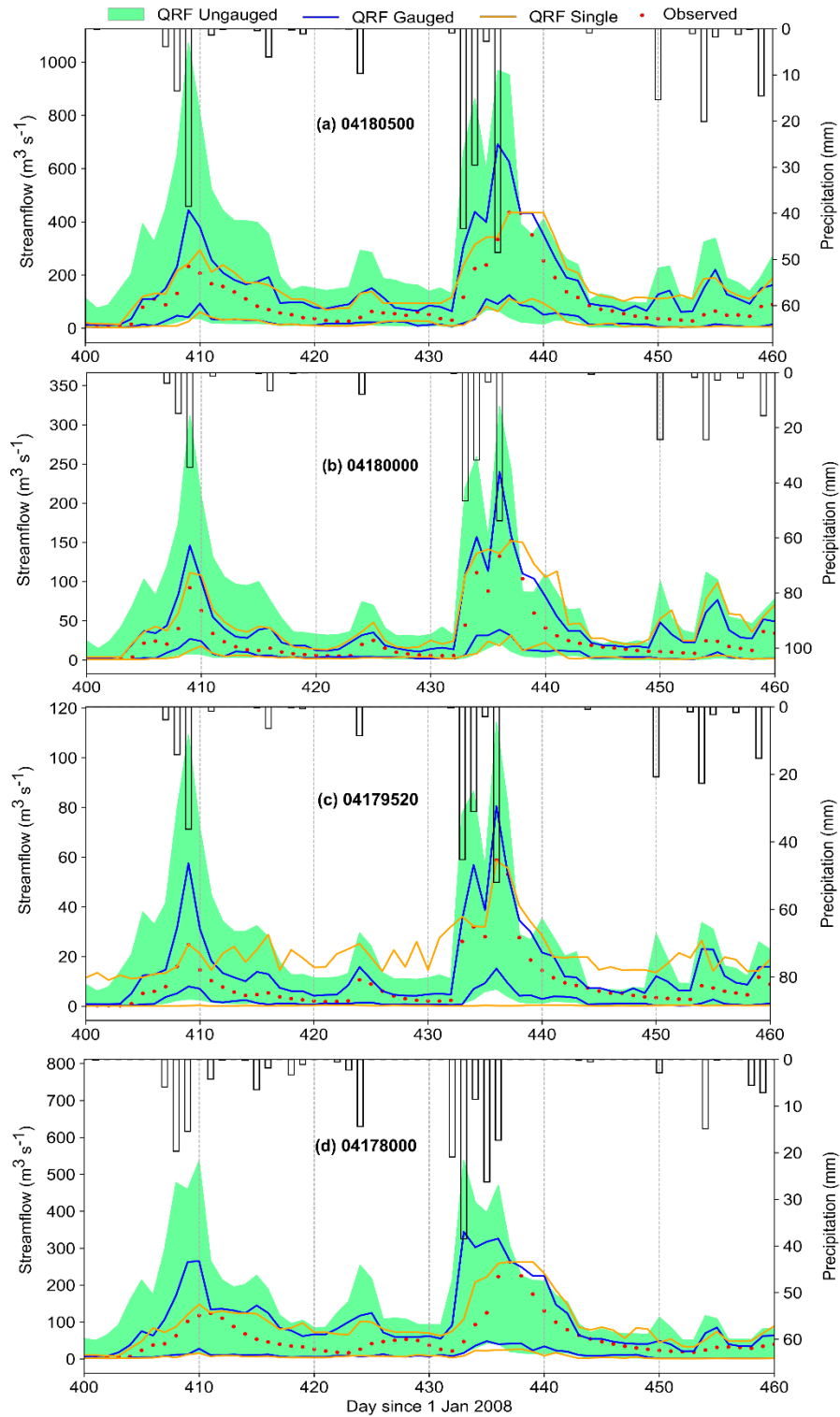
779 3.5 Limits-of-acceptability (LOA) created using the QRF ungauged model

780 One of the major advantages of the QRF algorithm is that it can be used to construct LOAs at  
781 ungauged locations. Figure 13 shows the LOAs constructed by the QRF ungauged model, along  
782 with LOAs constructed by the other models for the sake of comparison. The LOAs obtained by  
783 the QRF-ungauged model were typically wider than the LOAs obtained by the other models. The

784 timing errors between LOAs and observed streamflow can also be observed for the QRF-ungauged  
785 model.

786 At the time step 406, there exists a small peak in LOAs along with a very small peak in observed  
787 streamflow, but the observed precipitation is either zero or negligible. This is clearly because of  
788 an error in precipitation magnitude. It is likely that there was a small amount of precipitation in  
789 the watershed which was not recorded by the precipitation gauges. There were a few other such  
790 events where very small observed precipitation corresponded to a significant observed streamflow  
791 resulting in very high runoff ratios (as discussed above). Therefore, depending upon the  
792 precipitation magnitudes during current and previous time steps, QRF predicts a peak in  
793 streamflow. Such peaks would not have any impact on model inference in the sense that a  
794 hydrological model would not produce streamflow peaks in the absence of rainfall and the  
795 simulated streamflows would always be enveloped by the LOAs at these time steps.

796 Figure 6 shows that more than 60% of the multiplied peaks were enveloped by the QRF uncertainty  
797 bound even for 100% errors ( $f = 2$ ) for the ungauged model. The analysis suggests that LOAs  
798 obtained by the ungauged model are very conservative due to use of data from other watersheds.  
799 This is desirable when the LOAs are to be constructed at an ungauged location since we want to  
800 include a large number of rainfall-runoff behaviors to construct LOAs at an ungauged location.  
801 The results of this analysis are encouraging in terms of usefulness of QRF approach in creating  
802 LOAs at gauged and ungauged locations.



803 Figure 13. LOAs obtained by quantile random forest (QRF) in ungauged scenario (green), by  
 804 QRF in gauged-all scenario (blue), by QRF in gauged-single scenario (orange), along with  
 805 precipitation.  
 806



#### 807 4. Logic behind the proposed hypothesis

808 In this section, a mathematical argument is presented for using the DTs for constructing LoAs. We  
809 hypothesize that if *infinite* amount of hydrologic data are available, DT estimated LOA will reflect  
810 the effect of uncertainty due to errors in rainfall and streamflow measurements. Even if this is a  
811 hypothetical scenario (as infinite are never available), it serves to illustrate the usefulness of DTs  
812 in constructing LOAs and provides a theoretical basis. In practical cases, the DTs would also  
813 reflect variability due to other sources. As the number of calibration samples approaches *infinity*,  
814 the error incurred by a DT approaches optimal Bayes error (Denil et al., 2014) which is the  
815 irreducible part of the error due to inherent variability in the process and due to measurement errors  
816 (both epistemic and aleatoric). Assuming, for the sake of discussion, that there is no inherent  
817 variability in the hydrologic processes (more on this below), then errors incurred by a decision tree  
818 approach measurement error as the samples size increases. Thus, the results of Denil et al. (2014)  
819 suggest that decision tree can be used to account for measurement uncertainty, even if it holds only  
820 for the hypothetical case of infinite data. However, it may not be immediately clear how the  
821 uncertainty bounds obtained by decision trees represent measurement uncertainty in case of  
822 infinite sample size. Here, we answer this question and elucidate the logic behind the proposed  
823 hypothesis. A formal analysis of the proposed hypothesis is provided in Appendix A.

824 First, consider the case where only the streamflow measurements are uncertain, and the rainfall  
825 measurements are free of errors. Further, assume that the errors in streamflow measurements are  
826 unbiased. As the sample size increases, the diameter of each leaf node approaches zero, that is,  
827 predictor vectors contained in a leaf node are approximately equal (a formal proof of this statement  
828 if given in Appendix A). The true streamflow values corresponding to predictor vectors contained  
829 in a leaf node are approximately equal and any variations in the observed streamflow would be  
830 due to measurement errors. Thus, given an infinite sample, the minimum and maximum values  
831 contained in the leaf node represent lower and upper bounds over streamflow, and the difference  
832 between these bounds is due to measurement uncertainty. A formal analysis of this case is given  
833 in Section A.1.

834 Second, consider the case where only the rainfall measurements are uncertain, and the streamflow  
835 measurements are error free. In this case also, the diameter of a leaf node would approach zero  
836 (for the same reason as in the first case), and predictor vectors contained in a leaf node would be  
837 near identical, as the sample size approach infinite. But, due to measurement errors, the underlying  
838 true values of predictor vectors contained in a leaf node would be different (more precisely, the  
839 projections of predictor vectors on rainfall subspace will be different). Since there exists a  
840 streamflow value corresponding to each true predictor vector, the set of streamflow values  
841 corresponding to true predictor vectors in a leaf node would represent the effect of measurement  
842 uncertainty in predictor vector on streamflow. A formal analysis of the second case is given in  
843 Section A.2.

844 Third, consider the case where both rainfall and streamflow measurements are corrupted by errors.  
845 The logic behind this case is similar to the logic discussed above for the first and second cases. A  
846 formal analysis of this case is given in Section A.3.

847 Finally, we elaborate on inherent variability in hydrologic processes. The mathematical analyses  
848 provided above, and in the Appendix A, implicitly assume that the predictors variables used to  
849 train the decision tree are *complete* in the sense that predictor variables contain all the information  
850 that is required to predict streamflow. This, however, is not possible since the physical structure

851 of the watershed itself will be changing continuously, albeit only slowly with intermittent large  
852 disruptions, which will change the hydrologic response of the watershed. This can be referred to  
853 as the inherent uncertainty in hydrologic processes which is irreducible. Therefore, given an  
854 infinite sample, decision trees would also account for this inherent variability along with the  
855 measurement uncertainty.

856 Both measurement uncertainty and inherent variability are generally dominated by epistemic  
857 errors. Since, to construct LOAs, only the upper and lower bounds on errors are required for a  
858 given rainfall-runoff event, it is sufficient that the errors incurred in a given event fall in the range  
859 of the errors incurred from other similar events. Further, since the errors are epistemic and  
860 available data are finite in practice, it is possible that the errors of some events do not fall in the  
861 range of errors represented in the data; therefore, accommodation for such outliers needs to be  
862 made while using LOAs for model inference.

## 863 **5. Summary and Conclusions**

864 Separation of structural and measurement uncertainty was recognized as one of the twenty-three  
865 unsolved problems in hydrology by Bloschl et al. (2019). The only way to address this problem is  
866 to estimate measurement uncertainty before model calibration. This is a difficult task given that  
867 statistical properties of rainfall and streamflow measurement uncertainty are poorly understood,  
868 especially those of rainfall measurements. There exist two dominant philosophies to address this  
869 problem: (1) To assume statistical distributions over measurement uncertainty due to both rainfall  
870 and streamflow errors, and (2) To construct limits-of-acceptability (LOA) that provide some  
871 bounds on measurement uncertainty before any modeling. LOA has been used within the GLUE  
872 framework. However, both of these philosophies may also be combined together in Approximate  
873 Bayes Computation (ABC) framework. LOA can also be used in a purely Bayesian framework by  
874 defining a likelihood function that penalizes the simulations based on their deviations from the  
875 LOA. The aim of this paper was to test the capability of decision tree algorithms in creating LOAs  
876 that provide meaningful bounds on measurement uncertainty.

877 In this study, quantile random forest (QRF) method was used to construct LOAs. The advantages  
878 of the QRF method are as follows: (1) it can reflect the effect of both precipitation and streamflow  
879 measurement uncertainty, (2) it can account for timing errors in precipitation, (3) it can be applied  
880 at the timescale of available data, and (4) it can be used to construct LOAs at ungauged catchments.  
881 The results show that the LOAs obtained by using QRF enveloped the uncertainty bounds over  
882 streamflow observations. Measurement uncertainty in streamflow due to aleatory variability was  
883 found to be very small. It was shown that the statistical structure of QRF uncertainty bound was  
884 similar to an uncertainty bound obtained by propagating rainfall uncertainty through a hydrological  
885 model. Some observations include:

- 886 (1) Standard deviations of streamflow obtained by the QRF method increase with increasing  
887 value of observed streamflow.
- 888 (2) CVs of simulated rainfall time series and QRF uncertainty bound follow the same pattern:  
889 they decrease with increasing value of rainfall and streamflow, respectively.
- 890 (3) The general pattern of increase and decrease of width of uncertainty bound was similar for  
891 QRF and runoff ratio methods.

892 The QRF method does not contain any mechanism that induces the uncertainty bounds to follow  
893 any pre-determined patterns. Therefore, existence of these patterns suggests the QRF method is

894 able to identify *some* of the characteristics of measurement uncertainty from data. We cannot  
895 conclude that all the characteristics of measurement uncertainty were identified because QRF is  
896 unable to extract all the hydrological information from available data for the four SJRW  
897 watersheds used as test cases in this study. Indeed, this is likely to be the case for most watersheds  
898 since data on all the factors determining the hydrological response of a watershed are not available.

899 A clear timing error between observed streamflow and the LOAs obtained by the QRF method  
900 was observed in all four test watersheds (Figures 5 and 11). These timing errors are likely due to  
901 timing errors in precipitation data. If this is correct, one implication is that QRF can potentially  
902 capture timing errors in rainfall if data from other watersheds are used to construct LOAs. Another  
903 possibility is that data from other watersheds may have introduced disinformation into the LOAs.  
904 Therefore, it appears that LOAs should be constructed using data from several sets of watersheds  
905 so that the effect of both the potential timing errors and disinformation can be accommodated. This  
906 will, in general, mean a larger number of behavioral models and higher predictive uncertainty.  
907 Overall, the results of this paper are encouraging in the favor of using QRF approach for  
908 constructing LOAs at both gauged and ungauged locations.

909 In the *hypothetical* scenario, when infinite amount of hydrological data are available, the QRF  
910 algorithm can actually reflect the effects of measurement uncertainty. A mathematical analysis  
911 (Appendix A) has been presented to show this. For a finite sample size, the uncertainty bounds  
912 obtained by a decision tree include contributions from structural uncertainty (of QRF method)  
913 along with measurement uncertainty. This analysis used the following main assumptions to prove  
914 the proposed hypothesis:

- 915 (1) The relationship between predictor and response variables is one-to-one.
- 916 (2) The mapping between predictor and response variable is continuous.
- 917 (3) The errors in predictor and response variables are unbiased but otherwise the errors could  
918 be either aleatoric or epistemic.
- 919 (4) Error can be assumed independently and identically distributed within a leaf node.

920 We note that assumption 1 was made for mathematical convenience. A similar analysis can be  
921 carried out without this assumption.

922 A major advantage of QRF method (and indeed the LOA approach) is that it is a non-parametric  
923 approach for constructing LOAs without resorting to strong assumptions on the statistical nature  
924 of streamflow and rainfall measurement errors. Thus, the QRF method offers promise as a  
925 powerful tool in hydrological model inference.

926 Rainfall-runoff data may also contain disinformative periods. To identify disinformation and  
927 biases, one requires physical understanding of the rainfall-runoff processes. Runoff ratio method  
928 is an example of using process-based knowledge to identify biases, but it is not valid for baseflow  
929 dominated catchments and cannot be applied at ungauged locations. Moreover, runoff ratio method  
930 can identify the effect of errors in terms of streamflow volume – it cannot identify timing errors.  
931 QRF method addresses these limitations of the runoff ratio method. QRF will not explicitly  
932 identify disinformative periods, but it will likely define LOAs for the disinformative periods such  
933 that a good model would not be rejected because of these periods.

934 Further, as mentioned above, it is possible that data from other watersheds introduce  
935 disinformation into the constructed LOAs. An interesting future problem in this respect would be

936 to combine QRF method with catchment similarity analysis such that data from only the  
 937 watersheds which are known to be hydrologically similar to the parent watershed (where LOAs  
 938 are be constructed) are used. This would potentially reduce the disinformation introduced by the  
 939 data from other catchments while yielding meaningful LOAs. This technique can be particularly  
 940 useful for prediction in ungauged basins. QRF method already uses catchment characteristics (in  
 941 the form of spatially averaged indices such as mean slope, mean soil properties etc.) to identify  
 942 similar catchments. This technique has been applied in this paper. However, better methods based  
 943 on hydrologic process understanding (e.g., Wagener et al., 2007) would be more effective in  
 944 identifying the similar catchments.

945 One can also use other ML algorithms for creating LOAs in addition to the QRF method. Given  
 946 the finite amount of data in practical applications, different algorithms would extract different  
 947 information from available data and hence a different estimate of LOAs will be obtained. A  
 948 combination of these different LOAs will be more desirable for model inference (a problem to be  
 949 explored in future).

#### 950 **Data availability**

951 All the data used in this work are publicly available and can be downloaded from the DOI  
 952 [https://zenodo.org/record/7697209#.ZAJT\\_xh\\_MKUK](https://zenodo.org/record/7697209#.ZAJT_xh_MKUK)

#### 953 **Acknowledgements**

954 An earlier version of the paper was substantially revised based on the review comments of Keith  
 955 Beven. We are grateful to him for his insightful comments on the paper. Part of this manuscript  
 956 was prepared when AG was a doctoral candidate at Purdue University. The rest of the manuscript  
 957 was written when AG was a postdoctoral associate at DRI where he was supported by DRI's  
 958 Postdoctoral Support funds. This support is gratefully acknowledged.

#### 959 **Appendix A: Mathematical analysis of the proposed hypothesis**

960 In this section, a heuristic mathematical analysis in the support of the proposed hypothesis is  
 961 provided. The aim of the analysis is to clarify the assumptions behind the hypothesis and  
 962 limitations in practical implementation. Specifically, we show why the data in leaf nodes of a  
 963 decision tree can be used to capture measurement uncertainty and under what condition structural  
 964 uncertainty would be small. The analysis is divided into three parts for convenience: (1) when  
 965 measurement errors occur in streamflow measurements only, (2) when measurement errors occur  
 966 in rainfall measurements only, and (3) when both rainfall and streamflow measurements incur  
 967 errors. We note that the analysis provided below is valid for both aleatoric and epistemic errors.

##### 968 *A.1. Case 1: Only streamflow measurements are uncertain*

969 First, we provide the analysis of the proposed hypothesis under the restriction that only the  
 970 streamflow measurements contain errors and rainfall measurements are free of errors. Let  $\mathcal{X}$   
 971 denote the predictor space,  $\mathbf{x} \in \mathcal{X}$  denotes a point in the predictor space, and  $\mathcal{N}_d(\mathbf{x})$  denote the  $d$ -  
 972 neighborhood of  $\mathbf{x}$  in  $\mathcal{X}$  where  $d$  is a suitable distance metric. Further, let us define by  $\mathcal{Y}$  the set  
 973 containing error corrupted value of a response variable as

$$\mathcal{Y} = \{y(\mathbf{x}) | \mathbf{x} \in \mathcal{X}\}. \quad (\text{A1})$$

974 Since  $y(\mathbf{x})$  is an error corrupted value, it can be written as

$$y(\mathbf{x}) = y_t(\mathbf{x}) + \epsilon, \quad (\text{A2})$$

975 where  $y_t(\mathbf{x})$  denotes the true but unobserved value of the response variable and  $\epsilon$  denotes the  
 976 measurement error in  $y$ . Here,  $\epsilon$  represent a general error term which can be a function of  $\mathbf{x}$  and/or  
 977  $y$ .

978 The data contained in a leaf node of a decision tree may be approximated as a neighborhood of the  
 979 points close to its center. For example, if a leaf node constitutes the set  $\mathcal{X}_k = \{\mathbf{x}_i | \mathbf{x}_i \in \mathcal{X}\}_{i=1}^k$ , and  
 980 the point  $\mathbf{x}_m \in \mathcal{X}_k$  is close to its center; then  $\mathcal{X}_k$  can be treated as a neighborhood of  $\mathbf{x}_m$ . To define  
 981 a neighborhood, a distance metric is needed, and distance metric chosen defines the shape of  
 982 neighborhood. In the analysis presented below, a different distance metric might be required for  
 983 different leaf nodes of the decision tree. This does not pose any challenge to the generality of the  
 984 analysis. The approximation of a leaf node by the  $d$ -neighborhood is made for the sake of  
 985 mathematical convenience so that the analysis is manageable. Similar assumptions have been made  
 986 by other authors (e.g., Denil et al., 2014).

987 **Assumption 1.** The mapping between predictor and response variables is continuous.

988 **Assumption 2.** The relationship between probability distribution of  $\epsilon$  with  $\mathbf{x}$  and  $y$  does not change  
 989 significantly in a  $c$ -ball,  $\mathcal{B}_c(\mathbf{x})$ ,

$$\mathcal{B}_c(\mathbf{x}) = \{x_i | d(\mathbf{x}, x_i) \leq c\}, \quad (\text{A3})$$

990 where  $c$  is a sufficiently small number. In other words, the distribution of  $\epsilon$  changes slowly over  
 991  $\mathcal{X}$ .

992 **Assumption 3.** Without loss of generality, we assume that the relationship between true values of  
 993 predictor and true values of response variables is one-to-one. This assumption is also made for  
 994 analytical convenience.

995 **Assumption 4:** The expected value of  $\epsilon$  is zero.

996 **Assumption 5:** The response variable  $y$  varies smoothly with the predictor variable  $\mathbf{x}$ . This is  
 997 particularly true for rainfall runoff models where unit increase in rainfall can result in a maximum  
 998 of unit increase in streamflow, all else being equal.

999

1000 For every  $\mathbf{x}_d \in \mathcal{N}_d(\mathbf{x})$ , there exists a  $y_d \in \mathcal{Y}$  by definition of  $\mathcal{Y}$ . By virtue of Equation (A2),  
 1001  $y_d(\mathbf{x}_d) = y_t(\mathbf{x}_d) + \epsilon$ . Define  $\mathcal{Y}_d$  as

$$\mathcal{Y}_d = \{y_d(\mathbf{x}_d) | \mathbf{x}_d \in \mathcal{N}_d(\mathbf{x})\}, \quad (\text{A4})$$

1002 and define  $\mathcal{Y}_{d,t}$  as

$$\mathcal{Y}_{d,t} = \{y_t(\mathbf{x}_d) | \mathbf{x}_d \in \mathcal{N}_d(\mathbf{x})\}, \quad (\text{A5})$$

1003 Further, define the quantity

$$\bar{y}_d(\mathbf{x}) = \frac{1}{Vol\{\mathcal{N}_d(\mathbf{x})\}} \int y_d(\mathbf{x}) d\mathbf{x} \quad (\text{A6})$$

1004 **Assertion 1.** The quantity  $\bar{y}_d(\mathbf{x})$ , defined in Equation (A6), approaches the true value  $y_t(\mathbf{x})$  as the  
 1005 number of samples increases.

1006 The proof of this assertion, along with technical conditions, can be found in Brieman et al., (1984)  
 1007 and Denil et al., (2014). These references do not directly consider errors in measurement, but the

1008 proofs provided in these references are still valid provided assumption 4 holds. If assumption 4 is  
 1009 not valid, then the prediction error obtained by a decision tree approaches the optimal Bayes error.  
 1010 Note that the discrete version of the Equation (A6) is the response variable estimated by the RF  
 1011 algorithm. Therefore, the structural errors in RF estimate would decrease arbitrarily as the sample  
 1012 size increases.

1013 **Assertion 2.** The diameter of the  $\mathcal{Y}_{d,t}$  is small, if the sample size is large. In other words, the  
 1014 maximum difference between the  $y_t$  values contained in  $\mathcal{Y}_{d,t}$  would be small. Let this difference  
 1015 be denoted by  $dia(\mathcal{Y}_{d,t})$ .

1016 We note the following

- 1017 • a decision tree aims to create leaf nodes so as to minimize some measure of prediction
- 1018 error (such as mean-square error) on test set,
- 1019 • the estimated response by the decision tree is the average of the response values contained
- 1020 in a leaf node given by Equation (A6), and
- 1021 • the leaf nodes create a partition of the predictor space  $\mathcal{X}$ , i.e., the subsets created by the
- 1022 leaf nodes are disjoint and cover the predictor space.

1023 These requirements are met only if the quantity  $dia(\mathcal{Y}_{d,t}(\mathbf{x}))$  is small for each  $\mathbf{x}$ . (Here,  $\mathcal{Y}_{d,t}$  is  
 1024 denoted as a function of the argument  $\mathbf{x}$ .) For, consider  $n$  points  $\mathbf{x}_1, \mathbf{x}_2, \dots, \mathbf{x}_n \in \mathcal{X}$  that constitute  
 1025 the training set with corresponding neighborhoods  $N_d(\mathbf{x}_1), N_d(\mathbf{x}_2), \dots, N_d(\mathbf{x}_n)$ . Denote the  
 1026 number of leaf nodes created by the decision tree by  $m$ . Clearly,  $m \leq n$ . Further, consider the  
 1027 expression for mean-square error,

$$MSE_n = \frac{1}{n} \sum_{i=1}^n \{y(\mathbf{x}_i) - \bar{y}(\mathbf{x}_i)\}^2, \quad (\text{A7})$$

1028 where  $\bar{y}(\mathbf{x}_i)$  is estimated response given by Equation (23). The expression (A7) is minimized  
 1029 when each term in the summation is minimized.

1030 If  $m \ll n$ , there will be many out of  $n$  points that would fall into the same leaf node and, therefore,  
 1031 will have identical estimate of the response. Thus,  $MSE_n$  would not be minimized. This seems to  
 1032 imply that for  $MSE_n$  to be minimized we need  $m = n$ . Due to measurement errors, however,  
 1033 minimization of  $MSE_n$  on training set may not result in minimization of  $MSE_n$  on test set. And  
 1034 making  $m = n$  is likely to result in overfitting. Therefore, to satisfy the three conditions above),  
 1035 the value of  $m$  must be less than  $n$  but not much smaller than  $n$ . As  $n$  increases,  $m$  should also  
 1036 increase; otherwise,  $m$  would become much smaller than  $n$ . (Technically, this condition translates  
 1037 to the following:  $m \rightarrow \infty$  and  $m/n \rightarrow 0$ , as  $n \rightarrow \infty$ ). In decision tree language, as  $n$  increases, the  
 1038 predictor space would be split into smaller and smaller partitioning subregions, i.e., diameter of  
 1039 the leaf nodes would become smaller and smaller. Hence, it follows that  $dia(N_d) \rightarrow 0$ , as  $n \rightarrow \infty$ .

1040 If diameter of  $N_d(\mathbf{x})$  is small, then by assumption 5 and the assumption that values in  $N_d(\mathbf{x})$  are  
 1041 error free, the  $dia(\mathcal{Y}_{d,t})$  is also small.

1042 In summary, if the sample size is large, then the decision tree would be able to create small leaf  
 1043 nodes in order to minimize mean-square error. More technically, for  $n > N_a$ , and  $\delta > 0$

$$dia(\mathcal{Y}_{d,t}) < \delta, \quad (\text{A8})$$

1044 where  $N_a$  is some arbitrary large value.

1045 **Theorem 1.** The set  $\mathcal{Y}_d$  approximately captures measurement uncertainty in response variable if  
1046 the sample size is large.

1047 **Proof:** The minimum value contained in  $\mathcal{Y}_d$  is greater than or equal to  $\min(\mathcal{Y}_{d,t}) + \epsilon_l$  and the  
1048 maximum value contained in  $\mathcal{Y}_d$  is less than or equal to  $\max(\mathcal{Y}_{d,t}) + \epsilon_u$ . Here,  $\epsilon_l$  denotes a value  
1049 in the left tail of the distribution of  $\epsilon$  such that probability of  $\epsilon$  taking a value less than or equal to  
1050  $\epsilon_l$  is  $\gamma_l$ . Similarly,  $\epsilon_u$  denotes a value in the right tail of the distribution of  $\epsilon$  such that probability  
1051 of  $\epsilon$  taking a value greater than or equal to  $\epsilon_u$  is  $\gamma_u$ . Note that  $\epsilon_l$  and  $\epsilon_u$  are likely to be negative  
1052 and positive quantities, respectively.

1053 By assertion 2, the difference between  $\max(\mathcal{Y}_{d,t})$  and  $\min(\mathcal{Y}_{d,t})$  is small for large  $n$ , and,  
1054 therefore,

$$\min(\mathcal{Y}_{d,t}) \approx \max(\mathcal{Y}_{d,t}) \approx y_t(\mathbf{x}). \quad (\text{A9})$$

1055 Using Equation (A9), the minimum and maximum values contained in  $\mathcal{Y}_d$  may be approximated  
1056 by  $y_t(\mathbf{x}) + \epsilon_l$  and  $y_t(\mathbf{x}) + \epsilon_u$ . These lower and upper bounds represent the bounds on  
1057 measurement uncertainty due to errors in streamflow measurements. As sample size increases, the  
1058 probabilities  $\gamma_l$  and  $\gamma_u$  would approach zero, the approximation (A9) would become more accurate,  
1059 and, thus, the proposed hypothesis would become more accurate.

1060 This completed the analysis of the 1<sup>st</sup> case.

1061 In the preceding paragraph, we argued mathematically that as the sample size increases and the  
1062 neighborhood  $\mathcal{N}_d(\mathbf{x})$  becomes smaller, the set  $\mathcal{Y}_d$  represents measurement uncertainty in  $y$  more  
1063 accurately. In reality,  $\mathcal{N}_d(\mathbf{x})$  cannot be arbitrarily small and the sample size is finite – thus  $\mathcal{Y}_d$   
1064 represents both measurement and structural uncertainty. However, the structural uncertainty would  
1065 still be small if the sample size is large enough so as to create small leaf nodes (see Assertion 2  
1066 above and Equation (A8)). Practically speaking, one can aim only for the modest goal of obtaining  
1067 an uncertainty bound where majority of width is due to measurement uncertainty. Fortunately, this  
1068 is useful in practice in the construction of LOAs as it helps avoid type-1 errors (rejecting models  
1069 with good structures) at the cost of a few type-2 errors (accepting a few models with bad  
1070 structures). This is a desirable property of the LOAs (Beven, 2019).

1071 *A.2. Case 2: Only rainfall measurements are uncertain*

1072 Let  $\mathcal{X}$  denote the predictor space,  $\mathbf{x} \in \mathcal{X}$  denote a point in the predictor space, and  $\mathcal{N}_d(\mathbf{x})$  denote  
1073 the  $d$ -neighborhood of  $\mathbf{x}$  in  $\mathcal{X}$  where  $d$  is a suitable distance metric. Here,  $\mathbf{x}$  represents a vector  
1074 containing rainfall and other relevant predictor variables. Let  $\mathbf{x}_r$  denote the component of  $\mathbf{x}$   
1075 containing error corrupted current and time-lagged rainfall values.  $\mathbf{x}_r$  can be written as

$$\mathbf{x}_r = \mathbf{x}_{r,t} + \epsilon_{x,r}, \quad (\text{A10})$$

1076 where  $\mathbf{x}_{r,t}$  is the true value and  $\epsilon_{x,r}$  is the error in  $\mathbf{x}_r$ . Denote by  $\mathcal{Y}$  the set containing  $y$  values as  
1077 defined in Equation (A1).

1078 **Assumption 6:** The expected value of  $\epsilon_{x,r}$  is zero.

1079

1080 **Assumption 7:** We assume that the probability distribution of  $\epsilon_x$  varies slowly within  $\mathcal{N}_d(\mathbf{x})$ . The  
 1081 probability distribution of  $\epsilon_x$  can be assumed independent and identically distributed within  
 1082  $\mathcal{N}_d(\mathbf{x})$ .

1083 For each  $\mathbf{x} \in \mathcal{N}_d(\mathbf{x})$ , there exists a true value  $\mathbf{x}_t$  and corresponding to each  $\mathbf{x}_t$ , there exists a  $y_t$   
 1084 value. Thus, we can define a set  $\mathcal{Y}_d$  similar to that defined in Equation (A4), only difference being  
 1085 that the  $\mathbf{x}$  values are error corrupted in this case.

1086 **Assertion 3:** The diameter of  $N_d(\mathbf{x})$  approaches zero as the sample size increases.

1087 This assertion follows from the proof of assertion 2.

1088 **Assertion 4:** The true value of the values contained in  $\mathcal{N}_d(\mathbf{x})$  approximate the probability  
 1089 distribution of  $\mathbf{x}$ , for large sample large.

1090 Following assertion 3, it is reasonable to assume that values contained in  $N_d(\mathbf{x})$  are approximately  
 1091 equal, that is, any  $\mathbf{x}_d \in N_d(\mathbf{x})$  is approximately equal to  $\mathbf{x}$ . But the values contained in  $N_d(\mathbf{x})$  are  
 1092 error corrupted; therefore, the true value corresponding to any  $\mathbf{x}_d \in N_d(\mathbf{x})$  can be written as

$$\mathbf{x}_{d,t} = \mathbf{x}_d - \epsilon_x = \mathbf{x} - \epsilon_x. \quad (\text{A11})$$

1093 From Equation (A11), it is clear that  $\mathbf{x}_{d,t}$  is a random variable with mean value  $\mathbf{x}$  and larger  
 1094 moments defined by  $\epsilon_x$ . Hence, the assertion 4 follows.

1095 Corollary 1: The minimum and maximum values contained in  $\mathcal{N}_d(\mathbf{x})$  can be approximated by  $\mathbf{x} +$   
 1096  $\epsilon_{x,l}$  and  $\mathbf{x} + \epsilon_{x,u}$ , respectively. Here,  $\epsilon_{x,l}$  and  $\epsilon_{x,u}$  are defined similarly as  $\epsilon_l$  and  $\epsilon_u$  are defined in  
 1097 theorem 1. Again,  $\epsilon_{x,l}$  and  $\epsilon_{x,u}$  are likely to be negative and positive quantities, respectively.

1098 **Assertion 5:** There exists a one-to-one mapping between  $N_d(\mathbf{x})$  and  $\mathcal{Y}_d$ .

1099 It can be seen from Equation (A11) that there exists a *unique* true value corresponding to each  
 1100  $\mathbf{x}_d \in N_d(\mathbf{x})$ . For two values contained in  $N_d(\mathbf{x})$  to be identical, the value of  $\epsilon_x$  will have to be  
 1101 identical; but the probability of such an event is practically zero (less than some arbitrarily small  
 1102  $\delta > 0$  to be more precise).

1103 By assumption 3, there exists a one-to-one relationship between true value of predictor and  
 1104 response variables; therefore, there must exist a one-one mapping between  $N_d(\mathbf{x})$  and  $\mathcal{Y}_d$ .

1105 **Theorem 2:** The set  $\mathcal{Y}_d$  provides the effect of measurement uncertainty in rainfall on streamflow  
 1106  $y_t(\mathbf{x})$ .

1107 The truth in this assertion stems from one-to-one mapping between the elements of  $\mathcal{N}_d(\mathbf{x})$  and  $\mathcal{Y}_d$   
 1108 (Assertion 5). And since by assertion 4,  $\mathcal{N}_d(\mathbf{x})$  provides measurement uncertainty in  $\mathbf{x}$ ,  $\mathcal{Y}_d$  yields  
 1109 the effect of measurement uncertainty in  $\mathbf{x}$  on  $y(\mathbf{x})$ .

1110 The set  $N_d(\mathbf{x})$  contains several elements with approximately the same value  $\mathbf{x}$ . But these values  
 1111 are error corrupted; the underlying true values will differ due to measurement uncertainty in  $\mathbf{x}$ . For  
 1112 each unique true value in  $N_d(\mathbf{x})$ , there exists a unique value of  $y$  in  $\mathcal{Y}_d$ . When we observe an error  
 1113 corrupted value  $\mathbf{x}$ , the corresponding response can be any value contained in  $\mathcal{Y}_d$  depending upon  
 1114 the error in  $\mathbf{x}$ . Therefore, the LOA corresponding to  $\mathbf{x}$  should be  $(\min(\mathcal{Y}_d), \max(\mathcal{Y}_d))$ .

1115 This completes the analysis of 2<sup>nd</sup> case.



1116 The above analysis is valid in the case of large number of samples. With finite samples,  $\mathcal{Y}_d$  would  
 1117 capture measurement uncertainty and structural uncertainty because the diameter of  $N_d(\mathbf{x})$  would  
 1118 not be small. But a sufficiently large number of samples would result in small structural  
 1119 uncertainty.

1120 *A.3. Case 3: Both streamflow and rainfall measurements are uncertain*

1121 Here, we consider the case where both the rainfall and streamflow measurements are corrupted by  
 1122 errors. This case is a combination of case 1 and case 2. The notations and assumptions are same  
 1123 as in previous two cases. Consider  $\mathbf{x}_d \in N_d(\mathbf{x})$  and the corresponding response variable  $y_d \in \mathcal{Y}_d$ .  
 1124 The error corrupted  $\mathbf{x}_d$  and  $y_d$  can be represented by Equations (A2) and (A10), respectively.

1125 **Theorem 3.** The set  $\mathcal{Y}_d$  provides lower and upper measurement bounds due to errors in response  
 1126 measurements and the effect of errors in predictor measurements, if the sample size is large.

1127 From theorem 2, clearly  $\mathcal{Y}_{d,t}$  would yield the effect of errors in predictor variable measurements.  
 1128 Here,  $\mathcal{Y}_{d,t}$  is defined as in Equation (A5). Further, note that since response measurement is also  
 1129 error corrupted, the values contained in  $\mathcal{Y}_d$  can be written as

$$y_d(\mathbf{x}_d) = y_t(\mathbf{x}_d - \epsilon_x) + \epsilon(y_t), \quad (\text{A12})$$

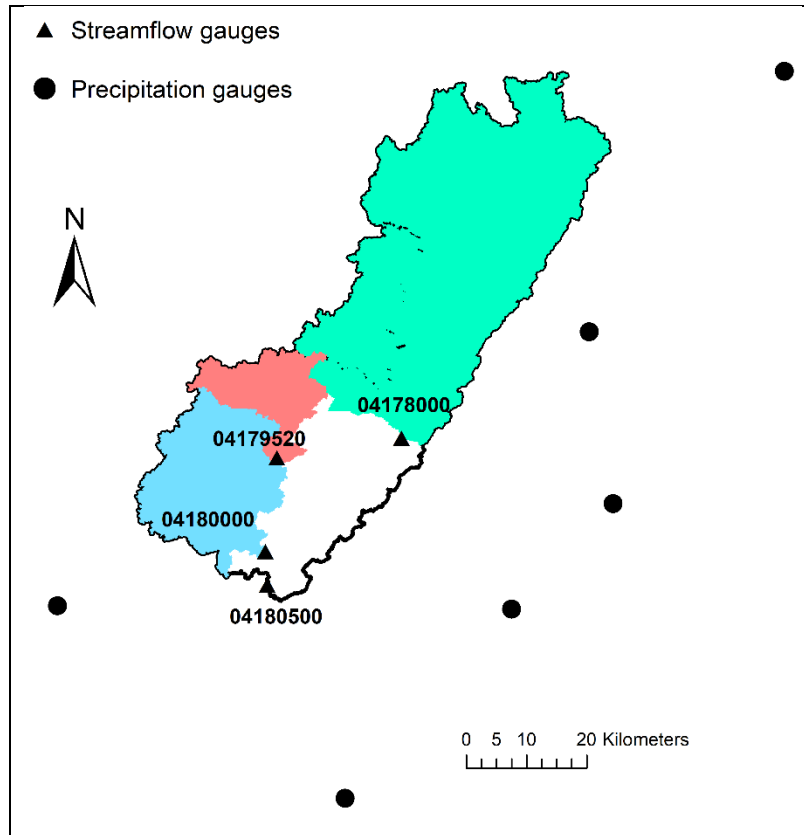
1130 where  $\mathbf{x}_d \in N_d(\mathbf{x})$  and  $y_d \in \mathcal{Y}_d$  are error corrupted values,  $y_t$  and  $\mathbf{x}_d - \epsilon_x$  are true values of  
 1131 predictor and response variables, respectively. The term  $\epsilon$  represents measurement error in  
 1132 response variable which is a function of  $y_t$ . Here,  $\epsilon$  cannot be assumed independent of  $y_t$  values  
 1133 since the variation of  $y_t$  within  $\mathcal{Y}_{d,t}$  is large in this case as opposed to that in case 1.

1134 Denote the set containing true value  $y_t$  corresponding to each true value in  $N_d(\mathbf{x})$  by  $\mathcal{Y}_{d,t}$ , as in  
 1135 Equation (A5). Then, the minimum and maximum values contained in  $\mathcal{Y}_d$  are  $\min(\mathcal{Y}_{d,t}) +$   
 1136  $\epsilon_l(\min(\mathcal{Y}_{d,t}))$  and  $\max(\mathcal{Y}_{d,t}) + \epsilon_u(\max(\mathcal{Y}_{d,t}))$ . Here,  $\epsilon_l(\min(\mathcal{Y}_{d,t}))$  is the value of  
 1137  $\epsilon(\min(\mathcal{Y}_{d,t}))$  in the left tail of the distribution such that probability of  $\epsilon(\min(\mathcal{Y}_{d,t}))$  taking a  
 1138 value less than  $\epsilon_l(\min(\mathcal{Y}_{d,t}))$  is  $\gamma_l$ . The term  $\epsilon_u(\max(\mathcal{Y}_{d,t}))$  is defined similarly. For large  
 1139 sample, the probability  $\gamma_l$  will approach 0. The quantities  $\min(\mathcal{Y}_{d,t}) + \epsilon_l(\min(\mathcal{Y}_{d,t}))$  and  
 1140  $\max(\mathcal{Y}_{d,t}) + \epsilon_u(\max(\mathcal{Y}_{d,t}))$  are lower and upper bounds of total measurement uncertainty due to  
 1141 errors in predictor and response variables.

1142 This completes the proof of case 3.

1143

1144 **Appendix B**



1145 Figure B1. Four sub watersheds located in St. Joseph River Watershed (SJRW) along with the  
 1146 precipitation gauges

1147 **References**

1148 Ammann, L., Fenicia, F., & Reichert, P. (2019). A likelihood framework for deterministic  
 1149 hydrological models and the importance of non-stationary autocorrelation. *Hydrology and Earth  
 1150 System Sciences*, 23(4), 2147-2172.

1151 Archuleta, C.M., Constance, E.W., Arundel, S.T., Lowe, A.J., Mantey, K.S., and Phillips, L.A.,  
 1152 2017, The National Map seamless digital elevation model specifications: U.S. Geological Survey  
 1153 Techniques and Methods, book 11, chap. B9, 39 p., <https://doi.org/10.3133/tm11B9>

1154 Bell, T. L. (1987). A space-time stochastic model of rainfall for satellite remote-sensing studies.  
 1155 *Journal of Geophysical Research: Atmospheres*, 92(D8), 9631-9643.

1156 Beven, K. (2005). On the concept of model structural error. *Water Science and Technology*, 52(6),  
 1157 167-175. Beven, K. (2019). Towards a methodology for testing models as hypotheses in the inexact  
 1158 sciences. *Proceedings of the Royal Society A*, 475(2224), 20180862.

1159 Beven, K., & Lane, S. (2019). Invalidation of models and fitness-for-purpose: A rejectionist  
 1160 approach. *Computer simulation Validation: Fundamental concepts, methodological frameworks,  
 1161 and philosophical perspectives*, 145-171.

1162 Beven, K., & Lane, S. (2022). On (in) validating environmental models. 1. Principles for  
 1163 formulating a Turing-like Test for determining when a model is fit-for purpose. *Hydrological  
 1164 Processes*, 36(10), e14704.

- 1165 Beven, K., & Westerberg, I. (2011). On red herrings and real herrings: disinformation and  
1166 information in hydrological inference. *Hydrological Processes*, 25(10), 1676-1680.
- 1167 Beven, K., Lane, S., Page, T., Kretzschmar, A., Hankin, B., Smith, P., & Chappell, N. (2022). On  
1168 (in) validating environmental models. 2. Implementation of a Turing-like test to modelling  
1169 hydrological processes. *Hydrological Processes*, 36(10), e14703.
- 1170 Beven, K., Smith, P., & Wood, A. (2011). On the colour and spin of epistemic error (and what we  
1171 might do about it). *Hydrology and Earth System Sciences*, 15, 3123-3133.
- 1172 Blöschl, G., Bierkens, M. F., Chambel, A., Cudennec, C., Destouni, G., Fiori, A., ... & Renner, M.  
1173 (2019). Twenty-three unsolved problems in hydrology (UPH)—a community perspective.  
1174 *Hydrological sciences journal*, 64(10), 1141-1158.
- 1175 Breiman, L., Friedman, J. H., Olshen, R. A., & Stone, C. J. (1984). *Classification and regression*  
1176 *trees*. Routledge.
- 1177 Brynjarsdóttir, J., & O’Hagan, A. (2014). Learning about physical parameters: The importance of  
1178 model discrepancy. *Inverse Problems*, 30(11), 114007.
- 1179 Coxon, G., Freer, J., Wagener, T., Odoni, N. A., & Clark, M. (2014). Diagnostic evaluation of  
1180 multiple hypotheses of hydrological behaviour in a limits-of-acceptability framework for 24 UK  
1181 catchments. *Hydrological Processes*, 28(25), 6135-6150.
- 1182
- 1183 de Oliveira, D. Y., & Vrugt, J. A. (2022). The treatment of uncertainty in hydrometric  
1184 observations: A probabilistic description of streamflow records. *Water Resources Research*,  
1185 58(11), e2022WR032263.
- 1186 Denil, M., Matheson, D., & De Freitas, N. (2014). Narrowing the gap: Random forests in theory  
1187 and in practice. In *International Conference on Machine Learning* (pp. 665-673). PMLR.
- 1188 Fernández, C., & Steel, M. F. (1998). On Bayesian modeling of fat tails and skewness. *Journal of*  
1189 *the American Statistical Association*, 93(441), 359-371.
- 1190 Fisher, R. A. (1956). *Statistical methods and scientific inference*. 3<sup>rd</sup> ed. McMillan, London.
- 1191 Friedman, J., Hastie, T., & Tibshirani, R. (2001). *The elements of statistical learning* (Vol. 1, No.  
1192 10). New York: Springer series in statistics.
- 1193 Gabellani, S., Boni, G., Ferraris, L., Von Hardenberg, J., & Provenzale, A. (2007). Propagation  
1194 of uncertainty from rainfall to runoff: A case study with a stochastic rainfall generator. *Advances*  
1195 *in Water Resources*, 30(10), 2061-2071.
- 1196 Gelman, A., & Rubin, D. B. (1992). Inference from iterative simulation using multiple sequences.  
1197 *Statistical Science*, 7(4), 457-472.
- 1198 Gong, W., Gupta, H. V., Yang, D., Sricharan, K., & Hero III, A. O. (2013). Estimating epistemic  
1199 and aleatory uncertainties during hydrologic modeling: An information theoretic approach. *Water*  
1200 *Resources Research*, 49(4), 2253-2273.

- 1201 Govindaraju, R. S. (2000). Artificial neural networks in hydrology. II: hydrologic applications.  
1202 *Journal of Hydrologic Engineering*, 5(2), 124-137.
- 1203 Gupta, A., & Govindaraju, R. S. (2022). Uncertainty quantification in watershed hydrology: Which  
1204 method to use? *Journal of Hydrology*, 128749.
- 1205 Gupta, A., Govindaraju, R. S., Morbidelli, R., & Corradini, C. (2022). The Role of Prior  
1206 Probabilities on Parameter Estimation in Hydrological Models. *Water Resources Research*,  
1207 e2021WR031291.
- 1208 Gupta, V. K., & Waymire, E. C. (1993). A statistical analysis of mesoscale rainfall as a random  
1209 cascade. *Journal of Applied Meteorology and Climatology*, 32(2), 251-267.
- 1210 Haario, H., Laine, M., Mira, A., & Saksman, E. (2006). DRAM: efficient adaptive MCMC.  
1211 *Statistics and Computing*, 16(4), 339-354.
- 1212 Herschy, R. (1993). The stage-discharge relation. *Flow Measurement and Instrumentation*, 4(1),  
1213 11-15.
- 1214 Iorgulescu, I., & Beven, K. J. (2004). Nonparametric direct mapping of rainfall-runoff  
1215 relationships: An alternative approach to data analysis and modeling? *Water Resources Research*,  
1216 40(8).
- 1217 Kavetski, D., Kuczera, G., & Franks, S. W. (2006a). Bayesian analysis of input uncertainty in  
1218 hydrological modeling: 1. Theory. *Water Resources Research*, 42(3).
- 1219 Kavetski, D., Kuczera, G., & Franks, S. W. (2006b). Bayesian analysis of input uncertainty in  
1220 hydrological modeling: 2. Application. *Water Resources Research*, 42(3).
- 1221 Kennedy, M. C., & O'Hagan, A. (2001). Bayesian calibration of computer models. *Journal of the  
1222 Royal Statistical Society: Series B (Statistical Methodology)*, 63(3), 425-464.
- 1223 Kiang, J. E., Gazoorian, C., McMillan, H., Coxon, G., Le Coz, J., Westerberg, I. K., ... & Mason,  
1224 R. (2018). A comparison of methods for streamflow uncertainty estimation. *Water Resources  
1225 Research*, 54(10), 7149-7176.
- 1226 Kratzert, F., Klotz, D., Herrnegger, M., Sampson, A. K., Hochreiter, S., & Nearing, G. S. (2019).  
1227 Toward Improved Predictions in Ungauged Basins: Exploiting the Power of Machine Learning.  
1228 *Water Resources Research*.
- 1229 Krueger, T., Freer, J., Quinton, J. N., Macleod, C. J., Bilotta, G. S., Brazier, R. E., ... & Haygarth,  
1230 P. M. (2010). Ensemble evaluation of hydrological model hypotheses. *Water Resources Research*,  
1231 46(7).
- 1232 Kuczera, G., & Parent, E. (1998). Monte Carlo assessment of parameter uncertainty in conceptual  
1233 catchment models: the Metropolis algorithm. *Journal of Hydrology*, 211(1-4), 69-85.
- 1234 Kuczera, G., Kavetski, D., Franks, S., & Thyer, M. (2006). Towards a Bayesian total error analysis  
1235 of conceptual rainfall-runoff models: Characterising model error using storm-dependent  
1236 parameters. *Journal of Hydrology*, 331(1-2), 161-177.
- 1237 Lamb, R., & Beven, K. (1997). Using interactive recession curve analysis to specify a general  
1238 catchment storage model. *Hydrology and Earth System Sciences*, 1(1), 101-113.

- 1239 Le Coz, J., Renard, B., Bonnifait, L., Branger, F., & Le Boursicaud, R. (2014). Combining  
1240 hydraulic knowledge and uncertain gaugings in the estimation of hydrometric rating curves: A  
1241 Bayesian approach. *Journal of Hydrology*, 509, 573-587.
- 1242 Lele, S. R. (2004). Evidence functions and the optimality of the law of likelihood. *The nature of*  
1243 *scientific evidence: Statistical, philosophical, and empirical considerations*, 191-216.
- 1244 Liu, Y., Freer, J., Beven, K., & Matgen, P. (2009). Towards a limits of acceptability approach to  
1245 the calibration of hydrological models: Extending observation error. *Journal of Hydrology*, 367(1-  
1246 2), 93-103.
- 1247 Mantoglou, A., & Wilson, J. L. (1982). The turning bounds method for simulation of random fields  
1248 using line generation by a spectral method. *Water Resources Research*, 18(5), 1379-1394.
- 1249 McMillan, H. K., Westerberg, I. K., & Krueger, T. (2018). Hydrological data uncertainty and its  
1250 implications. *Wiley Interdisciplinary Reviews: Water*, 5(6), e1319.
- 1251 McMillan, H., Krueger, T., & Freer, J. (2012). Benchmarking observational uncertainties for  
1252 hydrology: rainfall, river discharge and water quality. *Hydrological Processes*, 26(26), 4078-4111.
- 1253 Miller, J. W., & Dunson, D. B. (2019). Robust Bayesian inference via coarsening. *Journal of the*  
1254 *American Statistical Association*, 114(527), 1113-1125.
- 1255 Mishra, S. K., & Singh, V. P. (1999). Another look at SCS-CN method. *Journal of Hydrologic*  
1256 *Engineering*, 4(3), 257-264.
- 1257 Moulin, L., Gaume, E., & Obled, C. (2009). Uncertainties on mean areal precipitation: assessment  
1258 and impact on streamflow simulations. *Hydrology and Earth System Sciences*, 13(2), 99-114.
- 1259 Neyman, J., & Pearson, E. S. (1933). IX. On the problem of the most efficient tests of statistical  
1260 hypotheses. *Philosophical Transactions of the Royal Society of London. Series A, Containing*  
1261 *Papers of a Mathematical or Physical Character*, 231(694-706), 289-337.
- 1262 Nott, D. J., Marshall, L., & Brown, J. (2012). Generalized likelihood uncertainty estimation  
1263 (GLUE) and approximate Bayesian computation: What's the connection? *Water Resources*  
1264 *Research*, 48(12).
- 1265 Nott, D. J., Marshall, L., & Brown, J. (2012). Generalized likelihood uncertainty estimation  
1266 (GLUE) and approximate Bayesian computation: What's the connection? *Water Resources*  
1267 *Research*, 48(12).
- 1268 Pande, S. (2013a). Quantile hydrologic model selection and model structure deficiency  
1269 assessment: 1. Theory. *Water Resources Research*, 49(9), 5631-5657.
- 1270 Pande, S. (2013b). Quantile hydrologic model selection and model structure deficiency  
1271 assessment: 2. Applications. *Water Resources Research*, 49(9), 5658-5673.
- 1272 Petersen-Overleir, A., Soot, A., & Reitan, T. (2009). Bayesian rating curve inference as a  
1273 streamflow data quality assessment tool. *Water Resources Management*, 23(9), 1835-1842.
- 1274 Reichert, P., & Mieleitner, J. (2009). Analyzing input and structural uncertainty of nonlinear  
1275 dynamic models with stochastic, time-dependent parameters. *Water Resources Research*, 45(10).

- 1276 Reitan, T., & Petersen-Øverleir, A. (2009). Bayesian methods for estimating multi-segment  
1277 discharge rating curves. *Stochastic Environmental Research and Risk Assessment*, 23(5), 627-642.
- 1278 Renard, B., Kavetski, D., Kuczera, G., Thyer, M., & Franks, S. W. (2010). Understanding  
1279 predictive uncertainty in hydrologic modeling: The challenge of identifying input and structural  
1280 errors. *Water Resources Research*, 46(5).
- 1281 Renard, B., Kavetski, D., Leblois, E., Thyer, M., Kuczera, G., & Franks, S. W. (2011). Toward a  
1282 reliable decomposition of predictive uncertainty in hydrological modeling: Characterizing rainfall  
1283 errors using conditional simulation. *Water Resources Research*, 47(11).
- 1284 Royall, R. (2017). *Statistical evidence: a likelihood paradigm*. Routledge.
- 1285 Sadegh, M., & Vrugt, J. A. (2013). Bridging the gap between GLUE and formal statistical  
1286 approaches: approximate Bayesian computation. *Hydrology and Earth System Sciences*, 17(12),  
1287 4831-4850.
- 1288 Schoups, G., & Vrugt, J. A. (2010). A formal likelihood function for parameter and predictive  
1289 inference of hydrologic models with correlated, heteroscedastic, and non-Gaussian errors. *Water  
1290 Resources Research*, 46(10).
- 1291 Shortridge, J. E., Guikema, S. D., & Zaitchik, B. F. (2016). Machine learning methods for  
1292 empirical streamflow simulation: a comparison of model accuracy, interpretability, and  
1293 uncertainty in seasonal watersheds. *Hydrology & Earth System Sciences*, 20(7).
- 1294 Smith, T., Marshall, L., & Sharma, A. (2015). Modeling residual hydrologic errors with Bayesian  
1295 inference. *Journal of Hydrology*, 528, 29-37.
- 1296 Sturm, T. W. (2001). *Open channel hydraulics*. New York: McGraw-Hill.
- 1297 Tallaksen, L. M. (1995). A review of baseflow recession analysis. *Journal of Hydrology*, 165(1-  
1298 4), 349-370.
- 1299 Tompson, A. F., Ababou, R., & Gelhar, L. W. (1989). Implementation of the three-dimensional  
1300 turning bounds random field generator. *Water Resources Research*, 25(10), 2227-2243.
- 1301 Vrugt, J. A., & Beven, K. J. (2018). Embracing equifinality with efficiency: Limits of  
1302 Acceptability sampling using the DREAM (LOA) algorithm. *Journal of Hydrology*, 559, 954-971.
- 1303 Vrugt, J. A., & Sadegh, M. (2013). Toward diagnostic model calibration and evaluation:  
1304 Approximate Bayesian computation. *Water Resources Research*, 49(7), 4335-4345.
- 1305 Waymire, E. D., & Gupta, V. K. (1981a). The mathematical structure of rainfall representations:  
1306 1. A review of the stochastic rainfall models. *Water Resources Research*, 17(5), 1261-1272.
- 1307 Waymire, E. D., & Gupta, V. K. (1981c). The mathematical structure of rainfall representations:  
1308 3. Some applications of the point process theory to rainfall processes. *Water Resources Research*,  
1309 17(5), 1287-1294.
- 1310 Waymire, E.D., & Gupta, V. K. (1981b). The mathematical structure of rainfall representations:  
1311 2. A review of the theory of point processes. *Water Resources Research*, 17(5), 1273-1285.

- 1312 Westerberg, I. K., Guerrero, J. L., Younger, P. M., Beven, K. J., Seibert, J., Halldin, S., ... & Xu,  
1313 C. Y. (2011). Calibration of hydrological models using flow-duration curves. *Hydrology and Earth  
1314 System Sciences*, 15(7), 2205-2227.
- 1315 Zhang, B., & Govindaraju, R. S. (2000). Prediction of watershed runoff using Bayesian concepts  
1316 and modular neural networks. *Water Resources Research*, 36(3), 753-762.
- 1317 Zhang, B., & Govindaraju, R. S. (2003). Geomorphology-based artificial neural networks  
1318 (GANNs) for estimation of direct runoff over watersheds. *Journal of Hydrology*, 273(1-4), 18-34.